Regulated release of cryptococcal polysaccharide drives virulence and suppresses immune cell infiltration into the central nervous system

Steven T. Denham[1], Surbhi Verma[1,2], Raymond C. Reynolds[1], Colleen L. Worne[1], Joshua M. Daugherty[1], Thomas E. Lane[1], Jessica C.S. Brown[1,3]

[1]Division of Microbiology and Immunology, Pathology Department, University of Utah School of Medicine, Salt Lake City, UT, USA

[2]Present address: Biochemistry Department, University of Utah School of Medicine, Salt Lake City, UT, USA

[3]Correspondence: jessica.brown@path.utah.edu

Abstract:

Cryptococcus neoformans is a common environmental yeast and opportunistic pathogen responsible for 15% of AIDS-related deaths worldwide. Mortality primarily results from meningoencephalitis, which occurs when fungal cells disseminate from the initial pulmonary infection site and spread to the brain. A key *C. neoformans* virulence trait is the polysaccharide capsule. Capsule shields *C. neoformans* from immune-mediated recognition and destruction. The main capsule component, glucuronoxylomannan (GXM), is found both attached to the cell surface and free in the extracellular space (as exo-GXM). Exo-GXM accumulates in patient serum and cerebrospinal fluid at μg/mL concentrations, has well-documented immunosuppressive properties, and correlates with poor patient outcomes. However, it is poorly understood whether exo-GXM release is regulated or the result of shedding during normal capsule turnover. We demonstrate that exo-GXM release is regulated by environmental cues and inversely correlates with surface capsule levels. We identified genes specifically involved in exo-GXM release that do not alter surface capsule thickness. The first mutant, *liv7*Δ, released less GXM than wild-type cells when capsule is not induced. The second mutant, *cnag_00658*Δ, released more exo-GXM under capsule-inducing conditions. Exo-GXM release observed *in vitro* correlated with polystyrene adherence, virulence, and fungal burden during murine infection. Additionally, we find that exo-GXM reduces cell size and capsule thickness in capsule-inducing conditions, potentially influencing dissemination. Finally, we demonstrated that exo-GXM prevents immune cell infiltration into the brain during disseminated infection and highly inflammatory

69 intracranial infection. Our data suggest that exo-GXM performs a different role from
70 capsule GXM during infection, altering cell size and suppressing inflammation.
71
72 **Importance:**
73 *Cryptococcus neoformans* is a leading cause of life-threatening
74 meningoencephalitis in humans. *C. neoformans* cells produce an immunosuppressive
75 polysaccharide, glucuronoxylomannan (GXM), that is the main component of a
76 protective surface capsule. GXM is also released free into extracellular space as exo-
77 GXM, although the distinction between cell-attached GXM and exo-GXM has been
78 unclear. Exo-GXM influences the outcome of infection, is the basis for current
79 diagnostic tools, and has potential therapeutic applications. This study increases our
80 basic understanding of the fungal biology that regulates polysaccharide release,
81 suggesting that the release of cell-attached GXM and exo-GXM are distinctly regulated.
82 We also introduce a new concept that exo-GXM may alter cell body and capsule size,
83 thereby influencing dissemination in the host. Finally, we provide experimental evidence
84 to confirm clinical observations that exo-GXM influences inflammation during brain
85 infection.
86
87 **Introduction:**
88 *Cryptococcus neoformans* is a globally distributed saprophytic fungus found
89 associated with certain species of trees and bird droppings (1). However, in
90 immunocompromised humans *C. neoformans* acts as an opportunistic pathogen.
91 Cryptococcal infections are responsible for 15% of acquired immune deficiency

92 syndrome (AIDS) related deaths worldwide, with most cases occurring in sub-Saharan
93 Africa and Asia (2). Due to its global environmental distribution, human exposure to *C.*
94 *neoformans* is almost universal (1, 3). Infections begin when inhaled fungal spores or
95 desiccated yeast cells enter the lungs, where they are either cleared by the immune
96 system, or contained and persist for a decade or more (4). Upon patient
97 immunosuppression, *C. neoformans* cells can disseminate from the lungs to basically
98 any organ in the body (5). *C. neoformans* proliferates particularly well in the brain,
99 resulting in life-threatening meningoencephalitis (6). In fact, cryptococcal
100 meningoencephalitis is a primary cause of death among HIV-AIDS patients, with
101 mortality rates exceeding 50% in resource poor areas (2).
102 In contrast to many forms of bacterial and viral meningitis, cryptococcal
103 meningoencephalitis is associated with strikingly low levels of inflammation and
104 infiltrating immune cells into the central nervous system (CNS) of both human patients
105 and mouse models (7-11). This paucity of inflammation is linked to poorer clinical
106 outcomes, and subdued clinical signs that can delay treatment (9, 12, 13).
107 An essential factor for *C. neoformans* virulence is the conditional production of a
108 thick polysaccharide surface capsule, which can more than double the diameter of a *C.*
109 *neoformans* cell (14). The primary capsule constituent is glucuronoxylomannan (GXM),
110 which comprises approximately 90% of the capsule mass (15, 16). Surface capsule
111 plays a number of different roles during pathogenesis, protecting *C. neoformans* cells
112 from phagocytosis, complement, and oxidative stress (15, 17, 18). GXM also has
113 numerous immunomodulatory properties that facilitate fungal survival in the host (19).
114 Notably, GXM increases anti-inflammatory cytokine (IL-10) release while dampening

115 proinflammatory cytokine release (IL-12, IFN-γ TNF-α, IL-1B and IL-6) (20-23). GXM
116 disrupts antigen presentation by macrophages and dendritic cells, and can even induce
117 macrophage apoptosis, thereby diminishing T cell proliferation (21, 24-26). GXM can
118 also suppress leukocyte infiltration into sites of inflammation (27-29).

119 GXM is non-covalently attached to the cell surface during cell surface capsule
120 formation and maintenance (16). It is also found free within the extracellular milieu. This
121 exo-cellular GXM (exo-GXM) reaches mg/mL concentrations in laboratory growth
122 medium (30), and can be observed in the high μg/mL range in patient serum and
123 cerebrospinal fluid (10, 31). GXM serum titers in HIV-associated cryptococcosis patients
124 positively correlate with non-protective immune signatures and increased mortality (32).

125 Despite longstanding knowledge of the existence of exo-GXM, its connection to
126 cell-associated GXM and the mechanisms behind its release remain largely unclear.
127 One hypothesis has been that exo-GXM is shed mechanically from the cell surface
128 capsule (16, 33). Alternatively, it has been speculated that distinct mechanisms might
129 regulate the production of cell-associated and exo-GXM in response to environmental
130 cues (15, 16, 34). This latter hypothesis is supported by observations that cell-
131 associated and exo-GXM display different biophysical properties (34). Decreased
132 electromobility of exo-GXM under capsule inducing conditions indicates that these
133 differences could occur at the level of polymer length or branching (35-37).

134 Here we test the hypothesis that exo-GXM production is regulated by
135 environmental conditions. We find that exo-GXM production is inversely related to the
136 thickness of the cell surface-retained capsule and identify genes involved in these
137 processes. Exo-GXM production also correlates with virulence and reduces infiltration of

138 immune cells into the CNS during infection. Together, these data support the idea that
139 exo-GXM plays a critical but distinct role from cell surface GXM during infection.
140
141 **Results:**
142 *Environmental signals alter exo-GXM levels*
143 To investigate whether exo-GXM release is passive shedding of surface capsule
144 or regulated at some level, we cultured wild-type *C. neoformans* cells for 24 hours under
145 a variety of media conditions. We then measured capsule size and exo-GXM released
146 into the medium. We chose both non-capsule inducing media and a series of capsule
147 inducing media intended to produce a range of capsule induction. We harvested cells,
148 then stained with india ink to measure capsule thickness as the distance from the cell
149 wall to the outer capsule edge **(Fig. 1A)**. We filtered supernatant through a through a
150 0.22 μm filter to remove cells, then visualized with immunoblotting with the monoclonal
151 antibody (mAb) F12D2 to quantify exo-GXM release as relative staining intensity **(Fig.**
152 **1B)**. Exo-GXM band intensities were normalized to yeast nitrogen base (YNB) + 2%
153 glucose levels, which was the condition with the greatest observed levels of exo-GXM.
154 We found an inverse relationship between capsule thickness and exo-GXM, such
155 that cells growing in the strongest capsule inducing conditions, like 10% Sabouraud's
156 buffered to alkaline pH, produced the least amount of exo-GXM **(Fig. 1A,C)**. This
157 relationship held across other capsule inducing conditions, such as nitrogen and iron
158 limitation, that produce intermediate levels of both cell surface and exo-GXM.
159 GXM is an α-1,3-mannan backbone with branching glucuronic acid and xylose
160 residues and variable 6-*O*-acetylation on the backbone (38). *O*-acetylation varies across

strains, is not required for capsule formation, but significantly affects GXM's immunoreactive properties (38-40). Deletion of *CAS1*, which is required for *O*-acetylation, results in a hypervirulent phenotype (41). We analyzed the same conditioned media as in **Figure 1**, but used the mAb 1326 to detect GXM. MAb 1326 recognizes *O*-acetyl (+) GXM, but is unable to recognize *O*-acetyl (-) GXM. F12D2, on the other hand, recognizes both *O*-acetyl (+) and (-) GXM. Thus, 1326 staining intensity relative to F12D2 intensity reflects the relative proportion of *O*-acetyl (+) GXM present in the supernatant. We observed that 1326 staining relative to F12D2 staining increased under certain capsule inducing conditions (low nitrogen, low iron, and 10% Sabouraud's, pH 5-6), indicative of increased *O*-acetyl (+) GXM **(Fig. S1)**. These results demonstrate that environmental conditions may also influence GXM modification, specifically *O*-acetylation, with potential implications for immune recognition.

Identification of gene deletion mutants with reduced exo-GXM secretion under non-capsule inducing conditions.

We then identified mutants with reduced GXM production. We screened the *C. neoformans* partial knockout collection (CM18 background, 1200 targeted gene knockouts) (42) under YNB, which results in high exo-GXM production. We grew each strain for 24 hours at 37°C, removed the cells by centrifugation, then probed the conditioned medium for exo-GXM.

We searched the YNB-grown mutants for samples that produced less exo-GXM than wild-type cells. We then stained induced cell surface capsule (by growth in 10% Sabouraud's, pH 7.3) in this subset of mutants and eliminated any with a growth defect

and/or a substantial reduction (>25%) reduction in cell surface capsule thickness. We also stained for common pathogen-associated molecular patterns (PAMPs), such as exposed mannoproteins and chitin, which activate host immune responses (43). This left us with a single mutant, *cnag_06464*Δ, or *liv7*Δ, which we re-constructed in the KN99 genetic background (**Fig. 2**). Four other mutants (**Table S1**) exhibited a moderate defect in cell surface capsule in addition to their moderate defects in exo-GXM release. However, we focused on the *liv7*Δ mutant because of its ability to form wild-type levels of cell surface capsule.

The *LIV7* gene was previously identified in a screen for mutants deficient in growth in the lung (42). Liv7 is localized to the Golgi under capsule-inducing conditions (DMEM + 5% CO_2) (44). *liv7*Δ cells produce wild-type-like levels of cell surface capsule when grown in 10% Sabouraud's, pH 7.3 (**Fig. 2A,B**), but conditioned medium from *liv7*Δ cell cultures grown in YNB contains two-fold less GXM than conditioned medium from wild-type *C. neoformans* cell cultures (**Fig. 2C,D**). PAMP exposure is comparable to wild-type cells (**Fig. S2**).

Identification of gene deletion mutants with elevated exo-GXM secretion under strong capsule inducing conditions.

We next identified mutants that produced elevated levels of exo-GXM under capsule-inducing conditions, when exo-GXM production is very low. We again screened the *C. neoformans* knockout mutant collection (CM18 background), this time growing the mutants in YNB, then subculturing by diluting 1:100 into 10% Sabouraud's, pH 7.3, and growing 48 hours at 37°C. We again removed mutants that exhibited growth

207 defects, elevated PAMP exposure, and a substantial reduction (>25%) reduction in cell
208 surface capsule thickness. We found two groups of mutants: group #1 exhibited
209 approximately wild-type capsule thickness, while group #2 mutants had less-than-wild-
210 type levels of cell surface capsule (**Table S1**). We focused our subsequent experiments
211 on the mutant in gene *cnag_00658*, which produces cell surface capsule with the same
212 thickness as wild-type cells (**Fig. 3A,B**). As with *liv7*Δ, we re-constructed this mutant in
213 the KN99 genetic background and used those strains for all subsequent experiments.
214 As in the CM18 background, *cnag_00658*Δ cells in the KN99 background released
215 increased exo-GXM in 10% Sabouraud's, pH 7.3 **(Fig 3C,D)**. Unlike other mutants in
216 group #1, *cnag_00658*Δ cells produce the same levels of melanin and urease as wild-
217 type cells (**Fig. S2**).
218 The *CNAG_00658* gene encodes a predicted protein 624aa in length. It shares
219 N-terminal sequence homology with the *Schizosaccharomyces pombe* inner nuclear
220 membrane protein, IMA1 (615aa). *CNAG_00658*'s predicted gene product also has five
221 putative transmembrane domains that positionally align with the 5 transmembrane
222 domains of the *S. pombe* IMA1 protein. For these reasons, we propose to rename the
223 *CNAG_00658* gene*,* "*IMA1*". For the duration of this text, we will refer to "*cnag_00658*"
224 as "*ima1*".
225
226 *Changes in exo-GXM levels alter fungal cell adherence.*
227 We had thus far only assayed exo-GXM secretion during planktonic growth.
228 However, within its natural environment of soil and vegetable matter, *C. neoformans*
229 can form adherent biofilms (45). Previous work on cryptococcal biofilms has revealed

that a significant portion of the extracellular matrix is composed of GXM, and that it plays a critical role in adherence (46). Acapsular strains are unable to adhere to surfaces such as polystyrene, and the addition of anti-GXM antibodies to developing wild-type biofilms reduces their adherence (46). We speculated that exo-GXM may be incorporated into the extracellular matrix during sessile growth to provide community level structure, and that our exo-GXM mutants would display varying adherence corresponding to their exo-GXM secretion profiles.

To test this, we grew cells at a concentration of 10^6 cells/100ul in 96 well polystyrene plates at 37°C. After 48 hours, the wells were washed forcefully with PBS+0.1% tween-20 dispensed from an automated plate washer, resuspended in PBS containing XTT/menadione and left for 5 hours at 37°C. XTT is reduced by fungal cells to produce a colorimetric measure of metabolism that is highly correlative with viable cell count (47).

Wild-type, *cap60*Δ, *liv7*Δ#1 / #2, and *ima1*Δ#1 / #2 cells were assayed in both YNB and 10% Sabouraud's pH 7.3 to replicate planktonic non-capsule and capsule-inducing conditions respectively. The *cap60*Δ cells served as a negative control, as acapsular mutants are unable to adhere, likely due to their lack of surface and exo-GXM (46). We hypothesized that *liv7*Δ#1 / #2 cells would display reduced adherence in our assay due to the reduction in exo-GXM release we observed during planktonic growth. This was indeed the case, as we observed an approximately two-fold reduction in the ability of *liv7*Δ#1 / #2 cells to adhere in our assay **(Fig. 4A)**.

In contrast to YNB, *liv7*Δ#1 / #2 cells were able to adhere at wild-type levels when grown in 10% Sabouraud's pH 7.3, perhaps because our observations of

planktonic cells indicated that far less exo-GXM is released by both wild-type and *liv7*Δ#1 / #2 cells under these conditions **(Fig 4B)**. Similarly, *ima1*Δ#1 / #2 cells, which displayed elevated exo-GXM secretion under strong capsule inducing conditions, demonstrated six to eight-fold higher adherence than wild-type when grown in 10% Sabouraud's pH 7.3 **(Fig 4B)**. When grown in YNB, *ima1*Δ#1 / #2 cells still displayed increased adherence, but it was reduced to an approximately two-fold increase over wild-type **(Fig 4A)**. Altogether, these results suggest that the regulated secretion of exo-GXM may have a specialized role in an environmental setting by promoting the adherence of *C. neoformans* communities.

Host survival and fungal burden correlates with in vitro exo-GXM levels.

Next, we sought to use *liv7*Δ#1 / #2 and *ima1*Δ#1 / #2 as an opportunity to explore roles for exo-GXM during pathogenesis. We hypothesized that exo-GXM secretion would promote virulence through its immunomodulatory properties. Since *liv7*Δ#1 / #2 and *ima1*Δ#1 / #2 cells produce wild-type sized surface capsules in culture, we anticipated that *liv7*Δ#1 / #2 and *ima1*Δ#1 / #2 cells would allow us to assess the role of exo-GXM in pathogenesis, independent of surface capsule. We predicted that the reduction of *liv7*Δ#1 / #2 cells' ability to produce exo-GXM *in vitro* would result in reduced virulence. Similarly, we predicted that *ima1*Δ#1 / #2 cells, which show increased exo-GXM under capsule inducing conditions, would display heightened virulence.

We employed a murine model of disseminated cryptococcosis by inoculating C57BL/6NJ mice (Jackson Labs) intranasally with $2.5x10^4$ fungal cells per mouse. We

276 calculated survival as the time it took each mouse to reach 85% of their initial mass.
277 Consistent with our hypothesis, *in vitro* exo-GXM production inversely correlated with
278 host-survival. Wild-type KN99 infected mice reached endpoint a median of 20 days
279 post-inoculation (dpi). In contrast, *liv7*Δ#1 / #2-infected mice reached endpoint a median
280 of 22.5 dpi, and *ima1*Δ#1 / #2-infected mice a median of 18 dpi **(Fig. 5A)**. However, it is
281 important to note that all strains were sufficiently virulent to cause lethal infection at our
282 inoculating dose. This was not altogether unexpected, as the exo-GXM secretion
283 phenotypes for *liv7*Δ#1 / #2 and *ima1*Δ#1 / #2 cells were dependent on growth
284 conditions, and manifested as a gradient of exo-GXM production rather than complete
285 ablation or overexpression.
286 We also assessed fungal burden by plating homogenized organs for colony
287 forming unit (CFU) counts. Organ fungal burden followed the same trends as survival.
288 Mice inoculated with *liv7*Δ#1 / #2 cells consistently presented with lower fungal burden
289 in the lungs by day 10 post-inoculation **(Fig. 5B)**. Dissemination of *liv7*Δ#1 / #2 cells to
290 the spleen **(Fig. S3)** and brain **(Fig. 5C)** was also reduced compared to wild-type. In
291 contrast, mice inoculated with *ima1*Δ#1 / #2 cells suffered higher pulmonary fungal
292 burden compared to those inoculated with wild-type *C. neoformans* **(Fig. 5D)**.
293 Differences were present as soon as 3 days post-inoculation **(Fig. 5D)**. We also
294 observed a greater number of disseminated *ima1*Δ#1 / #2 cells in the liver and spleen
295 throughout the course of infection **(Fig. S3)**. *ima1*Δ#1 / #2 cells disseminated to the
296 brain earlier than wild-type cells, with some *ima1*Δ#1 / #2 infected mice showing CFUs
297 in the brain as early as 3 dpi **(Fig 5E)**. Total brain fungal burden in *ima1*Δ#1 / #2
298 infected mice trended higher than wild-type, with one independent gene deletion strain

299 achieving a statistically significant increase in fungal burden 10 dpi and beyond, despite
300 high variance in dissemination at the observed time points (**Fig. 5E)**. These results
301 suggest that time-to-endpoint for the mice was at least partially due to fungal lung
302 burden and extrapulmonary dissemination, both of which correlated with *in vitro* exo-
303 GXM secretion.

304 Since *in vitro* exo-GXM production by *ima1*Δ#1 / #2 and *liv7*Δ#1 / #2 cells
305 correlated with virulence *in vivo*, we examined whether or not the *in vitro* phenotypes
306 would translate to detectable differences in exo-GXM production in the host
307 environment. We analyzed the levels of GXM in the lungs, livers, spleens and brains of
308 infected mice by performing GXM ELISA's on 0.22 μm filtered organ homogenates.
309 Exo-GXM levels *in vivo* were highly variable, perhaps reflecting the heterogeneous host
310 environment or assay insensitivity **(Fig. S4)**. In spite of thisvariability, we detected
311 significant reductions in total exo-GXM in the lungs and extrapulmonary organs of
312 *liv7*Δ#1 / #2 infected mice at certain time points, with these trends becoming more
313 apparent as infection progressed **(Fig. S4A-D)**. Similarly, *ima1*Δ#1 / #2 infected mice
314 displayed increased total exo-GXM in the lungs, spleen and liver by 14 dpi **(Fig. S4E-**
315 **G)**. We did not observe any interpretable differences in exo-GXM levels on a per cell
316 basis (data not shown), possibly due to changing host conditions over the course of
317 dissemination or assay variability. Spread and/or clearance of exo-GXM within the host
318 likely also played a role, as the spleen and livers of infected mice had massively
319 increased exo-GXM levels on a per cell basis.

320 Also of note, is that we detected exo-GXM in extrapulmonary organs prior to
321 consistent detection of colony forming units (CFU) in those same organs **(Fig. S5)**. This

observation may be relevant for diagnosticians interested in detecting cryptococcal infection prior to dissemination in at-risk patient populations, as early diagnosis of cryptococcosis greatly improves outcomes (48).

Cell size shifts dramatically during the course of infection parallel to increases in exo-GXM.

We investigated whether or not *in vitro* capsule phenotypes for the mutants were recapitulated *in vivo*. We isolated cryptococcal cells from infected mice, fixed them with paraformaldehyde, and measured cell body diameter, cell surface capsule thickness, and total diameter (cell diameter including capsule) using india ink **(Fig. 1A)**.

In wild-type-infected mice, cell and capsule size in the lungs was a broad distribution that shifted significantly over the course of infection, as observed by others (49-51). Large cells were in high abundance early in infection, particularly at 3 dpi **(Fig. 6A)**. These cells were likely Titan cells, which are large, highly polyploid, and increase their size and ploidy through non-mitotic genome replication (14). However, as infection progressed, the frequency of large cells decreased. By 20 dpi, smaller cells around 10μm in total diameter dominated the lungs in number **(Fig. 6A)**. The cell body size and capsule thickness distributions experienced proportional shifts, such that overall cell size to capsule thickness ratios were maintained (**Fig. S6A,B**). In the brain, the distribution of cell and capsule size was much narrower and overlapped with the population of smaller cells in the lungs **(Fig. 6B)**.

When we compared the total cell diameter distributions of wild-type and the exo-GXM mutants in the lungs, there was no difference 3 dpi **(Fig. 6C,D)**. By an early time

345 point in dissemination (14 dpi), however, the frequency of smaller cells was higher in
346 *ima1*Δ#1 / #2 infected mice and lower in *liv7*Δ#1 / #2 infected mice, when compared to
347 wild-type **(Fig. 6E,F)**. The ratio of cell size to capsule thickness was similar amongst all
348 strains **(Fig. S6C).**

349 Due to this correlation between cell and capsule size and exo-GXM, we
350 hypothesized that levels of exo-GXM could influence cell and capsule size. To test this,
351 we grew cells in strong cell surface capsule-inducing medium (10% Sabouraud's, pH
352 7.3) with minimal exo-GXM release. After 24 hours growth at 37°C, we diluted the
353 cultures 1:2 in fresh medium and added 100 ng/ml, 10 µg/ml, or 50 µg/ml of purified
354 GXM. After an additional 24 hours growth, we measured cell and capsule size. We
355 found that both capsule thickness (**Fig. 7A**) and cell size (**Fig. S7A**) decreased in a
356 dosage-dependent manner. The greatest decrease was in capsule thickness, which
357 showed a decrease from a median of 4 µm in control cultures to 1.5 µm in cultures
358 treated with 50 µg/ml GXM, a decrease of 62.5%. 100 ng/ml showed a more modest
359 decrease, to a median capsule thickness of 3.6 µm (a 10% decrease). 50 µg/ml and 10
360 µg/ml GXM treatments also resulted in a change in cell size, from a median of 6.0 µm
361 for untreated cells to 4.5 µm and 5.3 µm, respectively. 100 ng/ml GXM did not result in a
362 decrease in cell size, despite the observed change in capsule thickness (**Fig. S7A**).

363 GXM purification can result in contamination by detergents from the purification
364 protocol (30). Thus, we performed the same experiment, but added conditioned medium
365 (from a YNB-grown culture) instead of purified GXM. 20%, 10%, or 1% final
366 concentration of conditioned medium resulted in decreases in both capsule thickness
367 and cell size (**Fig. 7B, Fig. S7**). These capsule and cell size changes also depended on

368 growth: if we did not add fresh medium along with purified GXM, capsule thickness and
369 cell size did not change (**Fig. S7**).

370 Altogether, these data suggest that changes to exo-GXM observed *in vitro* can
371 affect pathogenesis. Total exo-GXM secreted throughout infection correlated with
372 decreased survival, increased fungal burden and more rapid generation of smaller
373 (haploid) cells in the lungs, which appear more likely to disseminate due to their
374 dominant presence in extrapulmonary organs.

375

376 *Exo-GXM limits innate immune cell infiltration into the brain.*

377 In human patients, cryptococcal meningoencephalitis is associated with a striking
378 paucity of inflammation (9). The main driver of mortality, particularly in
379 immunocompromised patients, is thought to be excessive fungal burden and GXM
380 accumulation within the CNS, which leads to a devastating increase in intracranial
381 pressure (10). C57BL/6NJ mice infected with the highly virulent KN99 strain display a
382 similar paucity of brain inflammation, despite significant fungal presence. For instance,
383 when we histologically compared the brains of KN99 infected mice to mock-infected
384 animals, we could detect very little sign of infiltrating immune cells by H&E staining in
385 KN99-infected mice, despite local presence of fungi **(Fig. S8)**. This was true both early
386 (14 dpi) **(Fig. S8A,B)** and late (21 dpi) in disseminated infection **(Fig. S8C,D)**.
387 Considering its immunosuppressive nature, we hypothesized that GXM could very likely
388 play a role in limiting brain inflammation during infection. We correspondingly reasoned
389 that infection with *liv7*Δ#1 / #2 cells might result in increased immune infiltration into the
390 brain, due to *liv7*Δ#1 / #2 cell's reduced exo-GXM secretion.

391 In order to address this hypothesis, we harvested the brains of wild-type and
392 *liv7*Δ#1 / #2 infected animals at 20 days post-intranasal inoculation and analyzed
393 immune infiltration into the brain via flow cytometry. CD4+ **(Fig. 8A)** and CD8+ **(Fig. 8B)**
394 cells were scarce in both wild-type and *liv7*Δ#1 / #2-infected brains. These data suggest
395 that T cells do not significantly respond to brain invasion by *C. neoformans*. Innate
396 immune cells (macrophages/neutrophils) did show some response to wild-type *C.*
397 *neoformans* cells in the brain, but it was only slightly elevated when compared to mock-
398 infected animals **(Fig. 8C,D)**. This is in stark contrast to bacterial or viral meningitis,
399 which often show high levels of infiltrating neutrophils and macrophages (7, 8).
400 Infiltration of both macrophages and neutrophils was increased in *liv7*Δ#1 / #2 infected
401 brains **(Fig. 8C,D)**. These results suggest that exo-GXM likely plays an important role in
402 brain immunosuppression that is independent of surface capsule.
403 We next sought to determine if exo-GXM was sufficient to suppress immune
404 infiltration into the brain if we induced brain inflammation by direct intracranial
405 inoculation. We purified GXM from YNB-grown cultures using standard methods (30).
406 Since we detected GXM associated with the brain up to five days prior to the
407 appearance of CFU **(Fig. S5)**, we administered 200 µg of purified GXM daily by
408 intraperitoneal injection, beginning five days prior to inoculation **(Fig. 9A)**. Additional
409 mice were administered sterile PBS as a control. We then inoculated mice intracranially
410 with either wild-type KN99 or acapsular *cap60*Δ cells. Unsurprisingly, *cap60*Δ cells
411 elicited greater numbers of immune infiltration into the brain **(Fig. 9B,C)**, and achieved a
412 significantly lower fungal burden than wild-type *C. neoformans* **(Fig. 9D)**. However,
413 administration of GXM to mice infected with *cap60*Δ cells reduced immune infiltration

(CD45^{hi} cells) into the brain **(Fig. 9B,C and Fig. S9)**, and increased fungal burden when compared to PBS-treated mice **(Fig. 9D)**. These results demonstrate that in the context of an inflammatory infection, exo-GXM is sufficient to promote fungal survival in the brain, likely through the suppression of brain immune infiltration.

Discussion:

Surface capsule is critical for *C. neoformans* virulence. However, GXM that is not attached to the cell surface, or exo-GXM, accumulates to significant levels in laboratory culture and during infection (10, 30, 31). Our data strongly suggest that *C. neoformans* inversely regulates surface capsule formation and exo-GXM release according to environmental cues. Within our tested conditions, GXM was constitutively produced but alternately retained at the cell surface or released into the extracellular milieu. Previous findings have also indicated that exo-GXM release might be an active process. For instance, a study comparing the properties of exo-GXM and capsular GXM showed that despite sugar composition remaining the same, capsular GXM and exo-GXM manifested distinct biophysical and antigenic properties (34). Additionally, electromobility of exo-GXM decreases under capsule inducing conditions, implying that structural changes that influence capsule formation (35). We also observed that *O*-acetylation of GXM's mannose backbone changes with environmental conditions. These findings potentially suggest that differential regulation of surface capsule and exo-GXM could occur at the level of GXM polymer length and/or other modification. More work is required to elucidate biophysical differences between cell surface retained- and exo-GXM.

437 We identified genes that play a role in exo-GXM release. Deletion of *LIV7*
438 reduces exo-GXM release in rich growth medium when cell surface capsule does not
439 form, but does not affect capsule thickness. It has been previously demonstrated that
440 *LIV7* is important for virulence and likely functions in Golgi transport (42, 44). Our
441 second exo-GXM mutant, a deletion of the gene *IMA1*, increased exo-GXM release
442 under strong capsule inducing conditions without affecting capsule thickness. We used
443 these two exo-GXM mutants as tools to investigate the biological importance of exo-
444 GXM independent of surface capsule.
445 We first established a positive correlation of exo-GXM release with biofilm
446 adherence, suggesting that exo-GXM release during environmental growth may be
447 important for promoting community level structure and adherence. It would not be
448 surprising for there to be additional functions for exo-GXM in environmental settings.
449 In a murine infection model, we showed a correlation between elevated *in vitro*
450 exo-GXM levels, fungal burden and poor host survival. Other groups have also
451 connected varied exo-GXM release with changes to virulence. Analysis of a virulence-
452 associated transcriptional network map previously revealed a positive correlation with
453 exo-GXM release and mouse lung infectivity over 7 days (52). However, the
454 transcription factor mutants also had altered surface capsule thickness, which may have
455 influenced infectivity (52). Deletion of the flippase encoding gene *APT1* also resulted in
456 reduced *in vitro* exo-GXM release despite wild-type surface capsule. The knockout was
457 hypovirulent, but in contrast to our mutants, had reduced surface capsule thickness *in*
458 *vivo* (53). Our results support these previous findings, and our new exo-GXM mutants
459 are a powerful tool for investigating exo-GXM because they do not suffer any alterations

460 to additional virulence factors. Our data also provide additional support for a model in
461 which regulated release of exo-GXM enhances virulence independent of surface
462 capsule.

463 Interestingly, exo-GXM also correlated with changes in cell body and capsule
464 size distributions in the lungs. In wild-type *C. neoformans* infected animals, fungal cell
465 body size and capsule thickness decreased over the course of infection, as exo-GXM
466 levels increased. Correspondingly, increased GXM levels in the mouse lungs positively
467 correlated with an increased frequency of smaller cells at an early time point in
468 dissemination. *C. neoformans* cells in the brain and other extrapulmonary organs are
469 much smaller than the lungs (**Fig. 6B** and (50, 54, 55)), suggesting that the emergence
470 of smaller cells in the lungs is an important step in dissemination. The addition of
471 purified GXM to *C. neoformans* cells growing in capsule-inducing media was sufficient
472 to decrease cell body size and capsule thickness in a growth-dependent manner (**Fig.**
473 **7**). These data suggest that exo-GXM may actually provide a concentration-dependent
474 signal to *C. neoformans* cells that reduces cell size and capsule thickness. In the lungs,
475 this mechanism may be a contributing factor in the generation of small cells with a
476 greater propensity for dissemination.

477 There is large body of literature demonstrating immunosuppressive properties for
478 GXM (19). We focused on the brain, as cryptococcal meningoencephalitis is the leading
479 cause of death in cryptococcosis patients and is characterized by low levels of
480 inflammation (9). Here, we observed that deleting a gene required for wild-type levels of
481 exo-GXM release *in vitro* (*LIV7*) altered the host immune response to *C. neoformans*
482 brain infection. Mice infected with *liv7*Δ cells had increased macrophages and

483 neutrophils infiltrating the brain, compared to wild-type infected mice. Furthermore,
484 administration of purified GXM was sufficient to reduce brain infiltrating immune cells in
485 the context of acapsular *C. neoformans* infection. These data echo a previous study that
486 showed GXM could reduce early infiltration of neutrophils in a model of acute bacterial
487 meningitis (56). Our results suggest that exo-GXM is an actively secreted virulence
488 factor that may influence cell morphology to facilitate dissemination, and is capable of
489 distally suppressing immune infiltration into the brain.
490

491 **Funding information**
492 This work was supported by a startup grant from the Pathology Department at the
493 University of Utah to J.C.S.B. and NIH R01 NS041249 to T.E.L.
494

495 **Figure 1: Levels of detectable exo-GXM negatively correlate with capsule**
496 **thickness under a variety of media conditions.** To generate conditioned media, we
497 normalized 24 hour cultures by volume, then passed the supernatants through a 0.22
498 μm filter to remove fungal cells. **(A)** Representative image of cell/capsule
499 measurements used in this study. **(B)** We tested supernatants for free GXM ("exo-
500 GXM") by blotting and probing with the F12D2 anti-GXM mAb. See Materials and
501 Methods for further details. A representative blot showing relative levels of exo-GXM
502 collected from cells cultured for 24 hours under a variety of capsule and non-capsule
503 inducing conditions. **(C)** Intensity of exo-GXM bands relative to YNB+2% glucose exo-
504 GXM (blue bars) were quantitated for three independent experiments and plotted next
505 to absolute measurements of capsule thickness (yellow bars) (n=30 cells). Data was

506 combined from three independent experiments. Bars represent the mean and error bars
507 represent the standard deviation (SD).
508
509 **Figure 2: Identification of a genetic mutant (*liv7*Δ) with reduced exo-GXM release,**
510 **but no observable changes to capsule thickness. (A)** Representative india ink
511 images of cells grown in 10% Sabouraud's dextrose pH 7.3 for 24 hours. Capsule
512 thickness was similar across KN99 wild-type (WT) cells, and cells from each
513 independent *liv7* deletion strain (*liv7*Δ#1 and *liv7*Δ#2) **(B)** Quantification of cell body
514 diameter and capsule thickness from three independent experiments (n=30 cells per
515 strain; bars represent mean with SD). **(C)** Conditioned media from wild-type and mutant
516 cultures grown in weak-capsule inducing conditions (YNB + 2% glucose) for 24 hours.
517 Blots were probed with anti-GXM antibody F12D2. **(D)** Quantification of blot signal
518 intensities shows reduced exo-GXM release by *liv7*Δ#1 / *liv7*Δ#2. Data was combined
519 from three independent experiments. P-values were calculated using a Mann-Whitney
520 test; bars represent mean with SD.
521
522 **Figure 3: Identification of a genetic mutant (*ima1*Δ) with increased exo-GXM**
523 **release, but no observable changes to capsule thickness. (A)** Representative india
524 ink images of cells grown in 10% Sabouraud's dextrose pH 7.3 for 24 hours. Capsule
525 thickness was similar across KN99 wild-type (WT) cells, and cells from each
526 independent *ima1* (also *cnag_00658,* see main text for details) deletion strain (*ima1*Δ#1
527 and *ima1*Δ#2). **(B)** Quantification of cell body diameter and capsule thickness from three
528 independent experiments (n=30 cells per strain; bars represent mean with SD) **(C)**

529 Conditioned media from cultures grown for 24 hours under strong capsule-inducing
530 conditions (10% Sabouraud's at pH 7.3). Blots were probed with anti-GXM antibody
531 F12D2. **(D)** Quantification of blot signal intensities shows increased exo-GXM release
532 by *ima1*Δ#1 / *ima1*Δ#2 (Combined data from three independent experiments. P-values
533 were calculated using a Mann-Whitney test; bars represent mean with SD.
534
535 **Figure 4: Mutants' alterations to exo-GXM release correlates with adherence.** 10^6
536 *C. neoformans* cells were seeded into individual wells of 96-well polystyrene plates and
537 incubated at 37°C. 48 hours later, the wells were washed to remove non-adhered
538 and/or weakly adhered cells before resuspension in XTT for colorimetric analysis of
539 metabolic activity as a proxy for viable cell count. **(A)** OD_{490} readings from cells grown in
540 YNB, normalizing to wild-type cell readings. *liv7*Δ#1 / #2 cell adherence was reduced
541 and *ima1*Δ#1 / #2 cell adherence was increased when compared to wild-type cells. **(B)**
542 OD_{490} readings from cells grown in 10% Sabouraud's pH7.3, normalizing to wild-type
543 cell readings. *ima1*Δ#1 / #2 cell adherence was increased when compared to wild-type
544 cells. Combined data from three independent experiments. P-values were calculated
545 using a Mann-Whitney test; bars represent mean with SD.
546
547 **Figure 5: Mutants' alterations to *in vitro* exo-GXM release correlate with changes**
548 **in survival and fungal burden during infection. (A)** C57BL/6NJ mice infected
549 intranasally with *ima1*Δ#1 / #2 (n=10 and n=10, respectively) reach endpoint
550 significantly sooner than wild-type infected mice (n=15). Wild-type infected mice
551 reached endpoint sooner than *liv7*Δ#1 / #2 (n=8 and n=14, respectively) infected mice.

552 Mock infected animals given sterile 1X PBS (n=5) did not show signs of disease 35
553 days post-inoculation. P-values were calculated using a Log-rank (Mantel-Cox) Test. **(B**
554 **and C)** Lung fungal burden is significantly higher in *ima1*Δ#1 / #2 (n=8 and n=8,
555 respectively) infected mice than wild-type infected mice (n=8) beginning at least 3 days
556 post-inoculation, while *liv7*Δ#1 / #2 infected mice (n=8 and n=8, respectively) show
557 decreased lung burden beginning between 10 days post-inoculation compared to wild-
558 type (n=12). **(D and E)** Dissemination to the brain trends higher in *ima1*Δ#1 / #2 infected
559 mice, and is significantly lower in *liv7*Δ#1 / #2 infected animals when compared to wild-
560 type P-values were calculated using a Mann-Whitney test.
561
562 **Figure 6: Cell size distributions over the course of infection.** We visualized fungal
563 cells from tissue homogenates (from infected mice in **Fig. 5B-E)** in india ink and
564 measured cell surface capsule size. Total diameter = cell + capsule diameter. Cell body
565 diameter = diameter from one edge of the cell wall to the other. Capsule thickness =
566 (total diameter -- cell body diameter)/2 **(Fig 1A)**. **(A)** Mean total cell diameter decreases
567 over time within the lungs of wild-type infected mice as the population shifts toward
568 smaller cells with smaller capsules (n=3-4 mice per time point, ≥120 cells per mouse).
569 **(B)** Disseminated cells found in the brain late in infection (20 dpi) overlay with the size
570 profile of smaller cells found in the lungs at the same time point. **(C and D)** Early after
571 inoculation (3 dpi) the distributions of both **(C)** *liv7*Δ#1 / #2 and **(D)** *ima1*Δ#1 / #2 cells
572 match that of wild-type in the lungs (n=3 mice, ≥50 cells per mouse). **(E and F)** At an
573 early point in dissemination (14 dpi), **(E)** *liv7*Δ#1 / #2 cell populations were of larger
574 average total cell diameter than wild-type *C. neoformans* cells in the lungs. **(F)** *ima1*Δ#1

575 / #2 cells were of smaller average total cell diameter than wild-type *C. neoformans* cells
576 (n=4 mice, ≥120 cells per mouse). P-values were calculated using a Mann-Whitney test.
577
578 **Figure 7**: **Treatment with GXM decreases capsule thickness.** We induced cell
579 surface capsule by growing cells 24 hours in 10% Sabouraud's pH 7.3, then added
580 various concentrations of either (**A**) purified GXM or (**B**) conditioned medium from a
581 YNB-grown culture of wild-type (KN99) *C. neoformans* cells. We find a dosage-
582 dependent decrease in capsule thickness following exposure to both purified GXM and
583 conditioned medium. Histograms contain data from four separate experiments, with at
584 least 60 cells measured per condition for each experiment. We also observed a
585 decrease in cell size (see **Fig. S7**) with GXM or conditioned medium treatment. P-
586 values were calculated using a Mann-Whitney test. Representative DIC images of **(C)**
587 untreated cells or **(D)** cells treated with 50 μg/ml GXM are shown.
588
589 **Figure 8: Mice infected with *liv7*Δ cells display increased innate immune infiltrate**
590 **in the brain.** Mouse brains were harvested late (20 dpi) in infection for flow cytometry
591 analysis of infiltrating immune cells. **(A)** $CD4^+$ T cells are scarce in both wild-type and
592 *liv7*Δ#1 / #2 infected brains. **(B)** $CD8^+$ T cells show a significant increase over wild-type
593 in *liv7*Δ#2 infected brains, but this was not replicated in *liv7*Δ#1 infected brains **(C)**
594 Macrophages ($CD45^{hi}F4/80^+$) and **(D)** neutrophils ($CD45^+Ly6G^+Ly6C^+$) are significantly
595 increased in the brains of *liv7*Δ#1 and #2 as compared to wild-type and mock-infected
596 brains. P-values were calculated using a Mann-Whitney test; bars represent the
597 median.

598

599 **Figure 9: Purified GXM is sufficient to suppress immune infiltration into the brain**
600 **in response to inflammation-inducing acapsular (*cap60*Δ) *C. neoformans*.** 6-week-
601 old C57Bl/6NJ mice were intracranially inoculated with 200 *cap60*Δ fungal cells in 30 µl
602 1X PBS. Beginning 5 days prior to inoculation, mice were administered intraperitoneal
603 injections of either 200 µg/mL GXM or 200 µl sterile PBS. On the day of inoculation,
604 mice were administered this treatment intravenously to ensure GXM would be present
605 in the blood-stream. At 3 dpi brains were harvested to determine fungal burden by
606 colony forming unit counts. Separate mice were sacrificed to analyze infiltrating immune
607 cells by flow cytometry. **(A)** Diagram of experimental procedures. **(B)** Mice infected with
608 *cap60*Δ displayed increased brain immune infiltrate ($CD45^{hi}$ cells) over wild-type
609 infected mice. Immune infiltration into the brains of *cap60*Δ infected mice was reduced
610 with the administration of GXM. **(C)** Representative flow plots for data shown in **(B)**. **(D)**
611 Mice infected with wild-type KN99 cells suffered increased fungal brain burden as
612 compared to mice infected with *cap60*Δ. Administration of GXM had no significant effect
613 on wild-type fungal burden, but resulted in significantly increased *cap60*Δ fungal burden
614 compared to *cap60*Δ-infected mice that did not receive GXM. P-values were calculated
615 using a Mann-Whitney test; bars represent the median.

616

617 **Table S1: Exo-GXM mutant screen results.** We screened the *C. neoformans* partial
618 knockout collection (CM18 background, 1200 targeted gene knockouts) under YNB,
619 which results in high exo-GXM release by wild-type cells, or 10% Sabouraud's pH7.3,
620 which results in low exo-GXM release. **(A)** Gene deletions which resulted in reduced

exo-GXM release in YNB after 24 hours but no growth defect or a substantial reduction (>25%) reduction in cell surface capsule thickness in 10% Sabouraud's pH 7.3. **(B)** Gene deletions which resulted in increased exo-GXM release in 10% Sabouraud's pH 7.3 after 24 hours. Class 1 gene deletion mutants had approximately wild-type-sized capsule thickness, while Class 2 mutants had reduced capsule thickness in 10% Sabouraud's pH 7.3.

Figure S1: Proportion of *O*-acetylated exo-GXM increases under stronger capsule inducing conditions. Conditioned media was collected and blotted as in **Fig. 1**. **(A)** Detection of GXM with an acetylation insensitive mAb (F12D2). **(B)** Detection of GXM from the same conditioned media with an acetylation-sensitive mAb (1326), which only recognizes *O*-acetylated GXM. Increased intensity indicates a greater level of *O*-acetylated GXM.

Figure S2: Canonical virulence determinants are intact in *liv7*Δ and *ima1*Δ cells. **(A)** Cells were grown overnight in YNB + 2%glucose, stained with the fluorescently labeled lectins concanavalin A (ConA-rhodamine) and wheat germ agglutinin (WGA-fluorescein) to estimate exposure of PAMPs on the cell surface. **(B)** Cells were grown overnight in YNB + 2%glucose, subcultured 1:100 in 10% Sabouraud's dextrose (10% sab), pH 7.3, and stained as in **(A)**. PAMP exposure was similar across all strains except *cap60*Δ, which lacks surface capsule. **(C)** 2.5×10^4 cells were spotted on L-3,4-dihydroxyphenylalanine (L-DOPA) agar to observe melanization 48 hours later. No obvious differences were detected. **(D)** 2.5×10^4 cells were spotted on Christensen's

644 urea agar to observe urease secretion 48 hours later as the change in agar coloration
645 from orange to pink. No obvious differences were detected.
646
647 **Figure S3: Liver and spleen fungal burden mostly correlates with *in vitro* exo-**
648 **GXM production.** These data are from the same experiments as in **Fig. 5**. **(A)** Fungal
649 burden in the livers of wild-type and *liv7*Δ#1 / #2 infected mice did not show consistent
650 differences over the course of infection. **(B)** Fungal burdens in *ima1*Δ#1 / #2 infected
651 livers were significantly higher than wild-type at 14 and 16 dpi. **(C)** Fungal burden in the
652 spleens of *liv7*Δ#1 / #2 infected mice was significantly lower than wild-type-infected
653 mice at 10 and 17 dpi. **(D)** Fungal burdens in *ima1*Δ#1 / #2-infected spleens were
654 significantly higher than wild-type infected mice at 14 and 16 dpi. P-values were
655 calculated using a Mann-Whitney test.
656
657 **Figure S4: Total free GXM levels in mice infected with *C. neoformans* exo-GXM**
658 **mutants.** Tissues from mice in **Fig. 3B-G** were homogenized and passed through a
659 0.22 μm filter to remove fungal cells, then GXM levels were measured by ELISA. **(A)**
660 Mouse lungs infected with *liv7*Δ#1 / #2 cells showed trends toward reductions in exo-
661 GXM levels when compared to wild-type, though statistical significance is not consistent
662 across independent gene deletions. **(B and C)** Mouse livers and spleens infected with
663 *liv7*Δ#1 / #2 cells showed reduced exo-GXM levels when compared to wild-type-infected
664 organs at 14 dpi. **(D)** Mouse brains infected *liv7*Δ#1 / #2 cells showed reduced exo-
665 GXM when compared to wild-type at 17dpi. **(E-G)** Exo-GXM was increased in *ima1*Δ#1 /
666 #2 infected lungs, livers, and spleens when compared to wild-type-infected organs at

14dpi. **(H)** No significant differences in exo-GXM were observed in *ima1*Δ#1 / #2 infected brains when compared to wild-type-infected brains. P-values were calculated using a Mann Whitney t test.

Figure S5: GXM appears in brains and spleens prior to the appearance of CFU. A time course of **(A)** fungal burden (CFU) and **(B)** GXM per organ following infection with wild-type *C. neoformans* shows that GXM is detectable in all organs by 3 dpi. CFU were not detectable in brains or spleens until 10 dpi. These data are the compiled wild-type infection data from **Fig. 5**, **Fig. S3**, and **Fig. S4**.

Figure S6: Distribution of *C. neoformans* cell body diameter and cell capsule thickness shift over the course of lung infection: These data are from the same experiments as **Fig. 6**. **(A)** Average *C. neoformans* cell body diameter in the lungs decreases over the course of infection (n=3-4 mice per time point, ≥120 cells per mouse). **(B)** Average capsule thickness in the lungs decreases over the course of infection at a rate similar to the change in cell body diameter (n=3-4 mice per time point, ≥120 cells per mouse). **(C)** The proportion of cell size to capsule thickness in the lungs is similar across wild-type, *liv7*Δ#1 / #2, and *ima1*Δ#1 / #2 cells in the lungs (n=4 mice, ≥120 cells per mouse). P-values were calculated using a Mann-Whitney test; error bars show medians.

Figure S7: **Treatment with GXM decreases cell size.** These data are from the same experiments as **Fig. 7**. Cell size decreases in a dosage-dependent manner with the

addition of (**A**) purified GXM at 50 µg/ml or 10 µg/ml, but not 100 ng/ml, even though capsule thickness decreased with the addition of 100 ng/ml GXM. (**B**) Conditioned medium at final concentrations of 20%, 10%, or 1% all decrease cell size. (**C**) Cell size and (**D**) capsule thickness do not change if cultures are not administered additional growth medium (10% Sabouraud's, pH 7.3) along with purified GXM, suggesting that these size changes are growth-dependent. P-values were calculated using a Mann-Whitney test.

Figure S8: Few immune cells infiltrate the brains of mice with disseminated cryptococcosis, despite high fungal burden. (A) Representative hematoxylin and eosin (H&E) and **(B)** consecutive Grocott's methenamine silver (GMS) stained midbrain sections early (14 dpi) in brain infection. We observed no signs of inflammatory infiltrate (excess purple hematoxylin staining) and minimal fungal presence (black silver staining; arrows point to fungi) early. **(C)** Representative H&E and **(D)** GMS stained cerebral cortex sections late (21 dpi) in brain infection. We continued to detect few signs of inflammatory infiltrate in H&E stained sections late in infection, despite significant and diffuse fungal presence within the meninges and parenchyma of the brain (arrows point to fungi).

Figure S9: Administration of purified GXM to mice inoculated intracranially with acapsular *C. neoformans* reduces brain immune infiltration. These data are from the same experiments as **Fig. 10**. Brain infiltrating immune cells were detected by flow cytometry and broken into **(A)** $CD45^{hi}F4/80^{+}$ macrophages, **(B)** $CD45^{+}Ly6G^{+}Ly6C^{+}$

713 Neutrophils, **(C)** $CD4^+$ (T cells), **(D)** $CD8^+$ (T cells). P-values were calculated using a
714 Mann-Whitney test.
715
716 **Methods:**
717 Conditioned media collection: *C. neoformans* cells were cultured overnight in
718 YNB+2%glucose at 30 °C before subculturing 1:100 in the desired medium. Culture
719 OD_{600} readings were taken 24 hours later and were normalized to the lowest measured
720 OD_{600}. Cells were pelleted by centrifugation at 3000xg for 5 min. The supernatant was
721 collected and passed through a 0.22 µm filter, yielding conditioned media.
722 The following growth media were used in this study: YPAD (20g/L bacto-peptone,
723 10g/L bacto-yeast extract, 2% glucose, 0.4g/L adenine sulfate). YPD (20g/L bacto-
724 peptone, 10g/L bacto-yeast extract, 2% glucose); YNB (Difco REF 291940) +2%
725 glucose; 25% YNB+2% glucose; Low iron media (LIM) (5g/L asparagine, 0.4g/L
726 K_2HPO_4, 0.1g $MgSO_4 \cdot 7H_20$, 0.5mg/L thiamine, 0.029mg/L boric acid, 1.88mg/L
727 $CuSO_4 \cdot 5H_20$, 0.36mg/L $MnCl_2 \cdot 4H_2O$, 0.021mg/L $ZnCl_2$, 0.18mg/L $NaMoO_4 \cdot 2H_20$,
728 0.05mg/L $CaCl_2 \cdot 2H_20$, 0.05mM bathophenanthroline disulfonic acid (BPDS), 1mM
729 EDTA, 2% glucose, 50mM MOPS pH 6.0), 10% Sabouraud's dextrose (Difco REF
730 238230) buffered with 50mM HEPES pH 8.0, HEPES pH 7.3, MOPS pH 6.0, or MES pH
731 5.0; YCB (Difco REF 239110) +5g/L urea; YCB+0.5g/L urea.
732
733 Conditioned media blots: 10 µl of conditioned media collected from *C. neoformans*
734 cultures were loaded into a 0.6% agarose gel and run at 33V for 18-20 hours at 0.5X
735 TBE. The gels were processed with a 10 minute depurination rinse in a 0.25M HCl

736 solution, followed by a 30 minute denaturation incubation in a 1.5M NaCl/0.5M NaOH
737 solution, and a 30 minute neutralization incubation in 1.5M NaCl/0.5M Tris-HCl, pH 7.5.
738 The gels were rinsed in distilled water following each incubation. Gel contents were
739 subsequently transferred to a positively charged membrane using a standard Southern
740 blot protocol with 10X SSC (saline-sodium citrate) in the reservoir. After overnight
741 transfer, the blots were soaked briefly in 2X SSC and dried. Blots were then blocked for
742 1 hour in 1X PBS+5% milk and incubated shaking overnight at 4 °C in 1X PBS+5% milk
743 with 1:40,000 anti-GXM monoclonal antibody. The following morning, blots were rinsed
744 3 times in 1X PBS, incubated 2 hours in 1X PBS+5% milk with 1:2500 goat anti-mouse
745 HRP antibody, and washed for 2.5 hours in 1X PBS+0.1% tween-20, changing the wash
746 buffer every 20 minutes. For imaging, blots were developed with Clarity Western ECL
747 substrate (BioRad Cat. 170-5061) and imaging on a BioRad Western Blot Imager. Anti-
748 GXM monoclonal antibodies used in this study: F12D2, 1326 (Thomas Kozel, University
749 of Nevada, Reno).
750
751 Cell measurements: *C. neoformans* cells collected from laboratory media were spun
752 down at 3000xg for 5 min, washed twice in 1X PBS and resuspended in 1X PBS. To
753 collect cells from infected mouse organs, 1 mL of organ homogenate was passed
754 through a 70 µm cell strainer (Fisher Cat. No. 22-363-548). At this junction, capsule
755 measurement methods were the same for both laboratory-grown and mouse-isolated *C.*
756 *neoformans* cells. Cells were fixed for 15 minutes in 2% paraformaldehyde before
757 washing twice with 1X PBS, and resuspending in 100 µl of 1X PBS. 4 µl of cell
758 suspension was mixed with 4 µl of india ink (Higgins No. 44201) on a microscope slide,

coverslipped and visualized. Successive, representative pictures were taken from the outside of the coverslipped area toward the middle, because smaller cells tended to spread towards the edges of the coverslip more so than larger cells. Total cell diameter was measured as the distance from one edge of the capsule to the opposite edge. Cell body diameter was measured as the distance from one edge of the cell wall to the opposite edge. Capsule thickness was calculated as the total cell diameter, minus the cell body diameter, and divided by two; (total cell diameter–cell body diameter)/2.

Screen for exo-GXM mutants: Cells were spotted from 96 well frozen stocks to omnitrays containing YPD agar, then grown for 48 hours at 30°C. Colonies are used to inoculate deepwell plates containing 1 ml yeast nitrogen base (YNB) per well. Deepwell plates were grown at 37°C for 48 hours with shaking (280 rpm). 10 µl of YNB culture were then used to inoculate 10% Sabouraud's (pH 7.3) cultures, which were then grown at 37°C for 48 hours with shaking. After growth, all cultures, either YNB or 10% Sabouraud's, pH 7.3, were harvested by centrifugation, then the supernatant was collected and stored for analysis.

We analyzed exo-GXM in YNB supernatants by dot blotting 4 µl of supernatant into each well of a dot blotter containing positively charged nylon membrane pre-soaked in 2X SSC, then applying vacuum. Membranes were air dried, then blocked and incubated with anti-GXM F12D2 antibody using standard procedures (see Materials and Methods section: *Conditioned media blots*). 10% Sabouraud's conditioned media samples were run on agarose gels and transferred to nylon membranes (see Materials and Methods section: *Conditioned media blots*).

Once we identified mutants with altered exo-GXM levels (decreased in YNB cultures or increased in 10% Sabouraud's, pH 7.3 cultures, we grew all mutants in 10% Sabouraud's, pH 7.3, then measured capsule thickness. Mutants with decreased cell surface capsule thickness (approximately 25% decrease compared to wild-type cells) were eliminated from further analysis. We then repeated the growth and exo-GXM blot for each strain. We normalized for cell density (to account for slow growing mutants), filtered the conditioned medium through a 0.22 μm filter to remove cells, and ran 10 μl of conditioned medium on an agarose gel using the procedure described in (see Materials and Methods section: *Conditioned media blots*). Finally, we stained for exposure of PAMPs such as chitin and mannoprotein (see Materials and Methods section: *Lectin Staining*) and removed mutants with increased exposure.

Lectin Staining: Cells grown for 24 hours in the appropriate media were pelleted, washed twice in 1X PBS and fixed for 12 minutes in 2% paraformaldehyde. Cells were then washed twice in 1X PBS and resuspended in 1X PBS. To an aliquot of cells, wheat germ agglutinin (WGA) conjugated to fluorescein (Vector Labs Cat. No. FL-1021) was added to a final concentration of 5 μg/ml, and incubated 30 minutes at room temperature with shaking. At the end of the WGA incubation, concanavalin A (ConA) conjugated to rhodamine (Vector Labs Cat. No. RL-1002) was added to a final concentration of 50 μg/ml. Cells were wash once in 1X PBS and imaged immediately.

Melanization and urease secretion: Cells grown overnight in YNB were washed twice in 1X PBS and resuspended to a final concentration of 2.5×10^6 cells/mL in 1X PBS. 10μl of

805 cell suspension was spotted onto L-DOPA containing agar or Christensen's urea agar
806 (Sigma 27048). Plates were checked daily for changes in melanization (brown/black
807 colonies on L-DOPA), and urease secretion (pink coloration surrounding colonies on
808 Christensen's urea).
809
810 GXM purification: GXM was purified as described previously (30). Briefly, 100 mL *C.*
811 *neoformans* cells were cultured in YNB + 2%glucose for 5 days at 30°C. Cultures were
812 centrifuged at 12,000xg for 15min and the supernatant collected. Polysaccharides were
813 precipitated from the supernatant overnight with the addition of 3 volumes of 95% EtOH
814 at 4 °C. The solution was then centrifuged at 15,000xg for one hour, resuspended in
815 0.2M NaCl and sonicated. After sonication, 3mg hexadecyltrimethylammonium bromide
816 (CTAB) (Fisher Cat. No. 227160) per 1 mg precipitate was slowly added to the solution
817 on low heat. After removing from heat, another 2.5 volumes of 0.5mg CTAB was added.
818 The solution was centrifuged at 11,000xg for 2 hours, and the pellet washed in 10%
819 EtOH to remove any remaining CTAB. After an additional centrifugation at 18,000xg,
820 the pellet was resuspended in 1M NaCl and sonicated for 2 hours. Once the GXM was
821 solubilized, it was dialyzed (3.5kDa cutoff) versus sterile distilled water and then
822 lyophilized. Purified, lyophilized GXM was stored at -80°C for subsequent use.
823
824 Adherence assay: We used a slightly modified protocol of biofilm formation and 2,3-Bis-
825 (2-Methoxy-4-Nitro-5-Sulfophenyl)-2*H*-Tetrazolium-5-Carboxanilide (XTT) analysis, as
826 described previously (46, 47). Briefly, 5 mL cultures were grown overnight in
827 YNB+2%glucose at 30 °C, pelleted, washed in 1X PBS, and resuspended in 1X PBS.

828 Cells were counted on a hemocytometer, diluted to 10^7 cells/mL in the appropriate
829 media and plated in 100 µl volumes in 96 µl polystyrene plates (avoiding edge wells).
830 Sterile media was plated as a negative control. Plates were incubated for 48 hours at
831 37 °C to allow for adherence and biofilm maturation. Plates were then washed 3 times
832 with 200 µl of 1X PBS+0.05% tween-20 using a BioTek 405 TS microplate washer set
833 to an intermediate flow rate. To determine the relative levels of cells that remained after
834 washing, we used the XTT reduction assay to quantitate metabolic activity as a proxy
835 for viable cell density. After plate washing, 100 µl of a solution containing 0.5g/L XTT
836 (Fisher Cat. No. X6493) and 4 µM menadione (Sigma Cat. No. 58-27-5) in acetone in
837 1X PBS was added to each well. Menadione was added to fresh XTT solution
838 immediately prior to adding the solution to a plate. Plates were incubated for 5 hours
839 before moving 80 µl supernatant aliquots to a new plate to read absorbance at 490nm.
840
841 Mice: For the intranasal infection model, we used ~8-week-old female C57BL/6NJ mice
842 (Jackson Labs). *C. neoformans* cells were harvested from overnight 30°C YPD cultures,
843 washed two times in 1X PBS, resuspended in 1X PBS, and then counted with a
844 hemocytometer to determine the inoculum. Mice were anesthetized with
845 ketamine/dexdomitor (mg/g) intraperitoneally before suspending them on horizontally
846 tied thread by their front incisors. Mice were kept warm with a heat lamp and inoculated
847 intranasally with $2.5x10^4$ *C. neoformans* cells in 50 µl 1X PBS. After 10 minutes, mice
848 were removed from thread and administered the reversal agent antisedan
849 (~0.0125mg/g) intraperitoneally. For survival analyses, mice were weighed daily and
850 euthanized by CO_2 asphyxiation and cervical dislocation, when they lost 15% of their

initial mass. Mice used to analyze fungal burden, capsule size, and GXM levels were euthanized by the same measures at designated time points. Mice used for flow cytometry analysis were anesthetized with isoflurane and intracardially perfused with cold 1X PBS before cervical dislocation and brain extraction.

For the intracranial infection model, we used ~6-week-old female C57BL/6NJ mice (Jackson labs). *C. neoformans* inoculum was prepared as described above. Prior to inoculation, mice were anesthetized with ketamine/dexdomitor, as above. Mice were inoculated intracranially with 200 *C. neoformans* cells in 30µl 1X PBS via a 26Gx1/2 needle. Animals were then administered antisedan to speed recovery.

Fungal Burden: Organs were harvested from euthanized mice, placed on ice, and homogenized with a Tissue Master Homogenizer (Omni International) in 5 mL 1X PBS. Serial dilutions of organ homogenates were plated on Sabouraud's dextrose agar with 10mg/mL gentamycin and 100 mg/mL carbenicillin, and stored at 30°C in the dark for three days. Resulting colony forming units (CFU) were then counted to determine fungal burden.

GXM ELISA: 500 µl of the same mouse organ homogenate used for CFU counts and *C. neoformans* cell measurements was collected and spun down at 3,000g for 5 minutes. The supernatant was then passed through a 0.22 µm filter to remove cells. GXM levels in the resulting were quantified using the ALPHA Cryptococcal Antigen enzyme immunoassay (IMMY Ref. CRY101). GXM purified from *C. neoformans* cultures was diluted to generate standard curves.

Histology: Perfused mouse brains were divided in half and fixed overnight in 4% paraformaldehyde. 8 µm thick sagittal slices were mounted on microscope slides and stored at -20 °C. Successive sections were stained with hematoxylin and eosin or Grocott's methenamine silver (ThermoFisher Scientific Cat. No. 87008).

Flow cytometry: Perfused mouse brains were collected in RPMI, ground gently to disperse tissue and spun in a 90% Percoll (Sigma Cat. No. P1644) with a 63% Percoll underlay to isolate leukocytes at the interface. Leukocytes were resuspended in FACS buffer (1X PBS, 1% bovine serum albumin), and stained with the appropriate fluorescently labeled antibodies. Labeled cells were fixed for 20 minutes in 4% paraformaldehyde before analysis on a LSRFortessa (BD Biosciences). Antibodies used in this study (eBiosciences): CD45-efluor450 (48-0451-82), CD4-APC (Cat. No. 17-0041-82), CD8-FITC (11-0081-82), F4/80-FITC (11-4801-82), Ly6G-FITC (11-5931-82), Ly6C-APC (17-5932-82).

References:

1. May RC, Stone NRH, Wiesner DL, Bicanic T, Nielsen K. 2016. Cryptococcus: from environmental saprophyte to global pathogen. Nat Rev Micro 14:106-117.
2. Rajasingham R, Smith RM, Park BJ, Jarvis JN, Govender NP, Chiller TM, Denning DW, Loyse A, Boulware DR. 2017. Global burden of disease of HIV-associated cryptococcal meningitis: an updated analysis. The Lancet Infectious Diseases 17:873-881.
3. Goldman DL, Khine H, Abadi J, Lindenberg DJ, Pirofski L-a, Niang R, Casadevall A. 2001. Serologic Evidence for Cryptococcus neoformans Infection in Early Childhood. Pediatrics 107:e66-e66.
4. Garcia-Hermoso D, Janbon G, Dromer F. 1999. Epidemiological Evidence for Dormant Cryptococcus neoformans Infection. Journal of Clinical Microbiology 37:3204-3209.

5. Idnurm A, Bahn Y-S, Nielsen K, Lin X, Fraser JA, Heitman J. 2005. Deciphering the Model Pathogenic Fungus Cryptococcus Neoformans. Nat Rev Micro 3:753-764.
6. Chen Y, Toffaletti DL, Tenor JL, Litvintseva AP, Fang C, Mitchell TG, McDonald TR, Nielsen K, Boulware DR, Bicanic T, Perfect JR. 2014. The Cryptococcus neoformans Transcriptome at the Site of Human Meningitis. mBio 5:e01087-13.
7. van de Beek D, de Gans J, Tunkel AR, Wijdicks EFM. 2006. Community-Acquired Bacterial Meningitis in Adults. New England Journal of Medicine 354:44-53.
8. Kim JV, Kang SS, Dustin ML, McGavern DB. 2009. Myelomonocytic cell recruitment causes fatal CNS vascular injury during acute viral meningitis. Nature 457:191-195.
9. Chuck SL, Sande MA. 1989. Infections with Cryptococcus neoformans in the Acquired Immunodeficiency Syndrome. New England Journal of Medicine 321:794-799.
10. Robertson EJ, Najjuka G, Rolfes MA, Akampurira A, Jain N, Anantharanjit J, von Hohenberg M, Tassieri M, Carlsson A, Meya DB, Harrison TS, Fries BC, Boulware DR, Bicanic T. 2014. Cryptococcus neoformans Ex Vivo Capsule Size Is Associated With Intracranial Pressure and Host Immune Response in HIV-associated Cryptococcal Meningitis. The Journal of Infectious Diseases 209:74-82.
11. Olszewski MA, Noverr MC, Chen G-H, Toews GB, Cox GM, Perfect JR, Huffnagle GB. 2004. Urease Expression by Cryptococcus neoformans Promotes Microvascular Sequestration, Thereby Enhancing Central Nervous System Invasion. The American Journal of Pathology 164:1761-1771.
12. Jarvis JN, Meintjes G, Bicanic T, Buffa V, Hogan L, Mo S, Tomlinson G, Kropf P, Noursadeghi M, Harrison TS. 2015. Cerebrospinal Fluid Cytokine Profiles Predict Risk of Early Mortality and Immune Reconstitution Inflammatory Syndrome in HIV-Associated Cryptococcal Meningitis. PLoS Pathogens 11:e1004754.
13. Boulware DR, Bonham SC, Meya DB, Wiesner DL, Park GS, Kambugu A, Janoff EN, Bohjanen PR. 2010. Paucity of Initial Cerebrospinal Fluid Inflammation in Cryptococcal Meningitis is associated with subsequent Immune Reconstitution Inflammatory Syndrome. The Journal of infectious diseases 202:962-970.
14. Zaragoza O, Nielsen K. 2013. Titan cells in Cryptococcus neoformans: Cells with a giant impact. Current opinion in microbiology 16:409-413.
15. O'Meara TR, Alspaugh JA. 2012. The Cryptococcus neoformans Capsule: a Sword and a Shield. Clinical Microbiology Reviews 25:387-408.
16. Doering TL. 2009. How Sweet it is! Cell Wall Biogenesis and Polysaccharide Capsule Formation in Cryptococcus neoformans. Annual review of microbiology 63:223-247.
17. Zaragoza O, Taborda CP, Casadevall A. 2003. The efficacy of complement-mediated phagocytosis of Cryptococcus neoformans is dependent on the location of C3 in the polysaccharide capsule and involves both direct and indirectC3-mediated interactions. European Journal of Immunology 33:1957-1967.

18. Zaragoza O, Chrisman CJ, Castelli MV, Frases S, Cuenca-Estrella M, Rodríguez-Tudela JL, Casadevall A. 2008. Capsule enlargement in Cryptococcus neoformans confers resistance to oxidative stress suggesting a mechanism for intracellular survival. Cellular microbiology 10:2043-2057.
19. Vecchiarelli A, Pericolini E, Gabrielli E, Kenno S, Perito S, Cenci E, Monari C. 2013. Elucidating the immunological function of the Cryptococcus neoformans capsule. Future Microbiology 8:1107-1116.
20. Vecchiarelli A, Retini C, Monari C, Tascini C, Bistoni F, Kozel TR. 1996. Purified capsular polysaccharide of Cryptococcus neoformans induces interleukin-10 secretion by human monocytes. Infection and Immunity 64:2846-2849.
21. Monari C, Bistoni F, Casadevall A, Pericolini E, Pietrella D, Kozel TR, Vecchiarelli A. 2005. Glucuronoxylomannan, a Microbial Compound, Regulates Expression of Costimulatory Molecules and Production of Cytokines in Macrophages. The Journal of Infectious Diseases 191:127-137.
22. Retini C, Kozel TR, Pietrella D, Monari C, Bistoni F, Vecchiarelli A. 2001. Interdependency of Interleukin-10 and Interleukin-12 in Regulation of T-Cell Differentiation and Effector Function of Monocytes in Response to Stimulation with Cryptococcus neoformans. Infection and Immunity 69:6064-6073.
23. Vecchiarelli A, Retini C, Pietrella D, Monari C, Tascini C, Beccari T, Kozel TR. 1995. Downregulation by cryptococcal polysaccharide of tumor necrosis factor alpha and interleukin-1 beta secretion from human monocytes. Infection and Immunity 63:2919-2923.
24. Retini C, Vecchiarelli A, Monari C, Bistoni F, Kozel TR. 1998. Encapsulation of Cryptococcus neoformans with Glucuronoxylomannan Inhibits the Antigen-Presenting Capacity of Monocytes. Infection and Immunity 66:664-669.
25. Vecchiarelli A, Pietrella D, Lupo P, Bistoni F, McFadden DC, Casadevall A. 2003. The polysaccharide capsule of Cryptococcus neoformans interferes with human dendritic cell maturation and activation. Journal of Leukocyte Biology 74:370-378.
26. Villena SN, Pinheiro RO, Pinheiro CS, Nunes MP, Takiya CM, DosReis GA, Previato JO, Mendonça-Previato L, Freire-de-Lima CG. 2008. Capsular polysaccharides galactoxylomannan and glucuronoxylomannan from Cryptococcus neoformans induce macrophage apoptosis mediated by Fas ligand. Cellular Microbiology 10:1274-1285.
27. Ellerbroek PM, Hoepelman AIM, Wolbers F, Zwaginga JJ, Coenjaerts FEJ. 2002. Cryptococcal Glucuronoxylomannan Inhibits Adhesion of Neutrophils to Stimulated Endothelium In Vitro by Affecting Both Neutrophils and Endothelial Cells. Infection and Immunity 70:4762-4771.
28. Dong ZM, Murphy JW. 1995. Intravascular cryptococcal culture filtrate (CneF) and its major component, glucuronoxylomannan, are potent inhibitors of leukocyte accumulation. Infection and Immunity 63:770-778.
29. Dong ZM, Murphy JW. 1996. Cryptococcal polysaccharides induce L-selectin shedding and tumor necrosis factor receptor loss from the surface of human neutrophils. Journal of Clinical Investigation 97:689-698.
30. Cherniak R, Morris LC, Anderson BC, Meyer SA. 1991. Facilitated isolation, purification, and analysis of glucuronoxylomannan of Cryptococcus neoformans. Infection and Immunity 59:59-64.

31. Jarvis JN, Percival A, Bauman S, Pelfrey J, Meintjes G, Williams GN, Longley N, Harrison TS, Kozel TR. 2011. Evaluation of a Novel Point-of-Care Cryptococcal Antigen Test on Serum, Plasma, and Urine From Patients With HIV-Associated Cryptococcal Meningitis. Clinical Infectious Diseases: An Official Publication of the Infectious Diseases Society of America 53:1019-1023.
32. Scriven JE, Graham LM, Schutz C, Scriba TJ, Wilkinson KA, Wilkinson RJ, Boulware DR, Urban BC, Lalloo DG, Meintjes G. 2016. A Glucuronoxylomannan-Associated Immune Signature, Characterized by Monocyte Deactivation and an Increased Interleukin 10 Level, Is a Predictor of Death in Cryptococcal Meningitis. The Journal of Infectious Diseases 213:1725-1734.
33. Buchanan KL, Murphy JW. 1998. What makes Cryptococcus neoformans a pathogen? Emerging Infectious Diseases 4:71-83.
34. Frases S, Nimrichter L, Viana NB, Nakouzi A, Casadevall A. 2008. Cryptococcus neoformans Capsular Polysaccharide and Exopolysaccharide Fractions Manifest Physical, Chemical, and Antigenic Differences. Eukaryotic Cell 7:319-327.
35. Yoneda A, Doering TL. 2008. Regulation of Cryptococcus neoformans Capsule Size Is Mediated at the Polymer Level. Eukaryotic Cell 7:546-549.
36. Cordero RJB, Frases S, Guimaräes AJ, Rivera J, Casadevall A. 2011. Evidence for Branching in Cryptococcal Capsular Polysaccharides and Consequences on its Biological Activity. Molecular microbiology 79:1101-1117.
37. de S. Araújo GR, Fontes GN, Leão D, Rocha GM, Pontes B, Sant'Anna C, de Souza W, Frases S. 2016. Cryptococcus neoformans capsular polysaccharides form branched and complex filamentous networks viewed by high-resolution microscopy. Journal of Structural Biology 193:75-82.
38. Kozel TR, Levitz SM, Dromer F, Gates MA, Thorkildson P, Janbon G. 2003. Antigenic and Biological Characteristics of Mutant Strains of Cryptococcus neoformans Lacking Capsular O Acetylation or Xylosyl Side Chains. Infection and Immunity 71:2868-2875.
39. Urai M, Kaneko Y, Ueno K, Okubo Y, Aizawa T, Fukazawa H, Sugita T, Ohno H, Shibuya K, Kinjo Y, Miyazaki Y. 2015. Evasion of Innate Immune Responses by the Highly Virulent Cryptococcus gattii by Altering Capsule Glucuronoxylomannan Structure. Frontiers in Cellular and Infection Microbiology 5:101.
40. Ellerbroek PM, Lefeber DJ, van Veghel R, Scharringa J, Brouwer E, Gerwig GJ, Janbon G, Hoepelman AIM, Coenjaerts FEJ. 2004. O-Acetylation of Cryptococcal Capsular Glucuronoxylomannan Is Essential for Interference with Neutrophil Migration. The Journal of Immunology 173:7513.
41. Janbon G, Himmelreich U, Moyrand F, Improvisi L, Dromer F. 2001. Cas1p is a membrane protein necessary for the O-acetylation of the Cryptococcus neoformans capsular polysaccharide. Molecular Microbiology 42:453-467.
42. Liu OW, Chun CD, Chow ED, Chen C, Madhani HD, Noble SM. 2008. Systematic genetic analysis of virulence in the human fungal pathogen Cryptococcus neoformans. Cell 135:174-188.
43. Willment JA, Brown GD. 2008. C-type lectin receptors in antifungal immunity. Trends in Microbiology 16:27-32.

44. Brown JCS, Madhani HD. 2012. Approaching the Functional Annotation of Fungal Virulence Factors Using Cross-Species Genetic Interaction Profiling. PLOS Genetics 8:e1003168.
45. Martinez LR, Casadevall A. 2015. Biofilm Formation by Cryptococcus neoformans. Microbiology Spectrum 3.
46. Martinez LR, Casadevall A. 2005. Specific Antibody Can Prevent Fungal Biofilm Formation and This Effect Correlates with Protective Efficacy. Infection and Immunity 73:6350-6362.
47. Pierce CG, Uppuluri P, Tristan AR, Wormley FL, Mowat E, Ramage G, Lopez-Ribot JL. 2008. A simple and reproducible 96 well plate-based method for the formation of fungal biofilms and its application to antifungal susceptibility testing. Nature protocols 3:1494-1500.
48. Vidal JE, Boulware DR. 2015. Lateral Flow Assay for Cryptococcal Antigen: an Important Advance to Improve the Continuum of HIV Care and Reduce Cryptococcal Meningitis-Related Mortality. Revista do Instituto de Medicina Tropical de São Paulo 57:38-45.
49. García-Barbazán I, Trevijano-Contador N, Rueda C, de Andrés B, Pérez-Tavárez R, Herrero-Fernández I, Gaspar ML, Zaragoza O. 2016. The formation of titan cells in Cryptococcus neoformans depends on the mouse strain and correlates with induction of Th2-type responses. Cellular Microbiology 18:111-124.
50. Okagaki LH, Strain AK, Nielsen JN, Charlier C, Baltes NJ, Chrétien F, Heitman J, Dromer F, Nielsen K. 2010. Cryptococcal Cell Morphology Affects Host Cell Interactions and Pathogenicity. PLoS Pathogens 6:e1000953.
51. Zaragoza O, García-Rodas R, Nosanchuk JD, Cuenca-Estrella M, Rodríguez-Tudela JL, Casadevall A. 2010. Fungal Cell Gigantism during Mammalian Infection. PLoS Pathogens 6:e1000945.
52. Maier EJ, Haynes BC, Gish SR, Wang ZA, Skowyra ML, Marulli AL, Doering TL, Brent MR. 2015. Model-driven mapping of transcriptional networks reveals the circuitry and dynamics of virulence regulation. Genome Research 25:690-700.
53. Rizzo J, Oliveira DL, Joffe LS, Hu G, Gazos-Lopes F, Fonseca FL, Almeida IC, Frases S, Kronstad JW, Rodrigues ML. 2014. Role of the Apt1 Protein in Polysaccharide Secretion by Cryptococcus neoformans. Eukaryotic Cell 13:715-726.
54. Rivera J, Feldmesser M, Cammer M, Casadevall A. 1998. Organ-Dependent Variation of Capsule Thickness in Cryptococcus neoformans during Experimental Murine Infection. Infection and Immunity 66:5027-5030.
55. Trevijano-Contador N, Rueda C, Zaragoza O. 2016. Fungal morphogenetic changes inside the mammalian host. Seminars in Cell & Developmental Biology 57:100-109.
56. Lipovsky MM, Tsenova L, Coenjaerts FEJ, Kaplan G, Cherniak R, Hoepelman AIM. 2000. Cryptococcal glucuronoxylomannan delays translocation of leukocytes across the blood–brain barrier in an animal model of acute bacterial meningitis. Journal of Neuroimmunology 111:10-14.

Figure 1

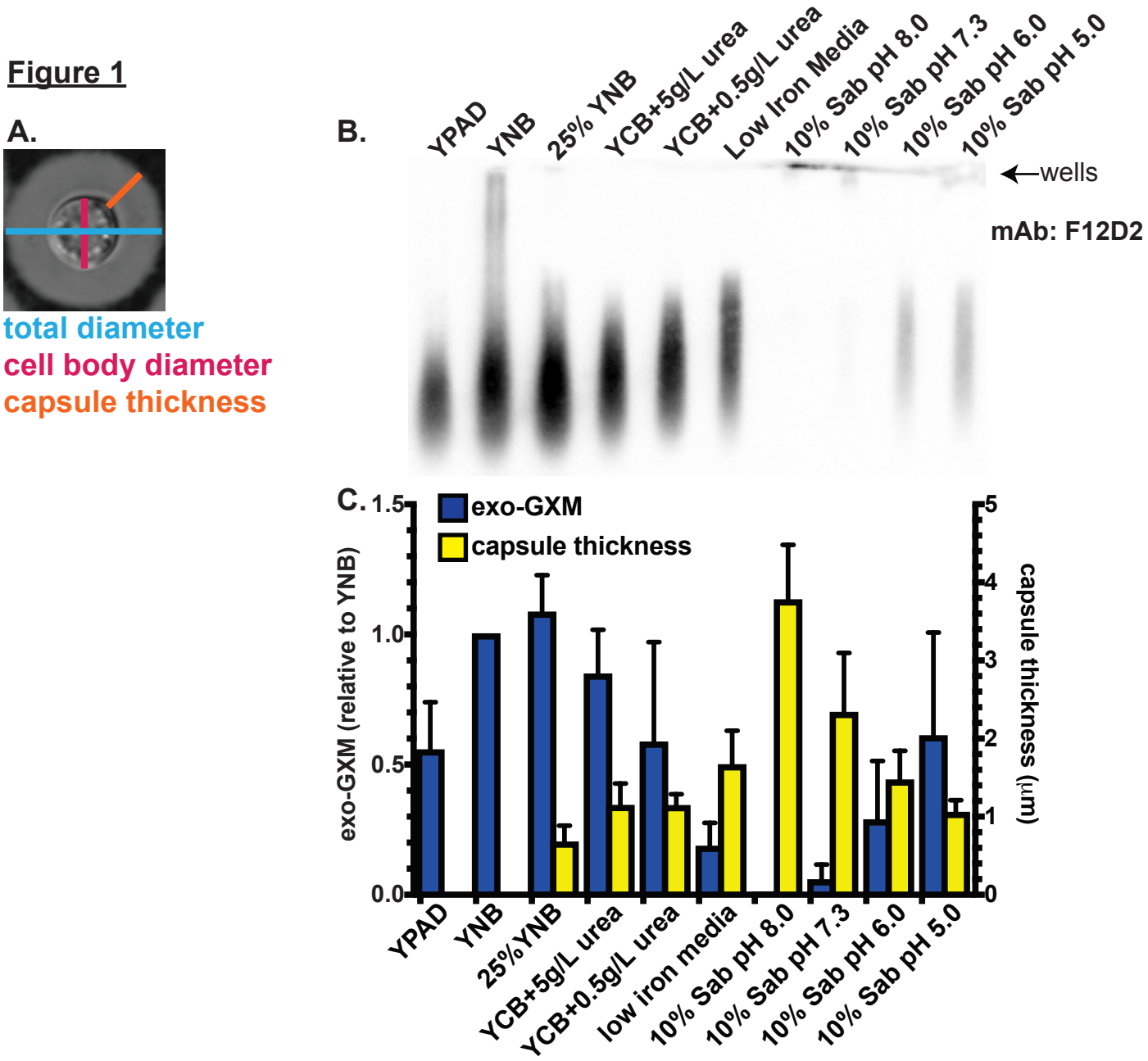

Figure 2

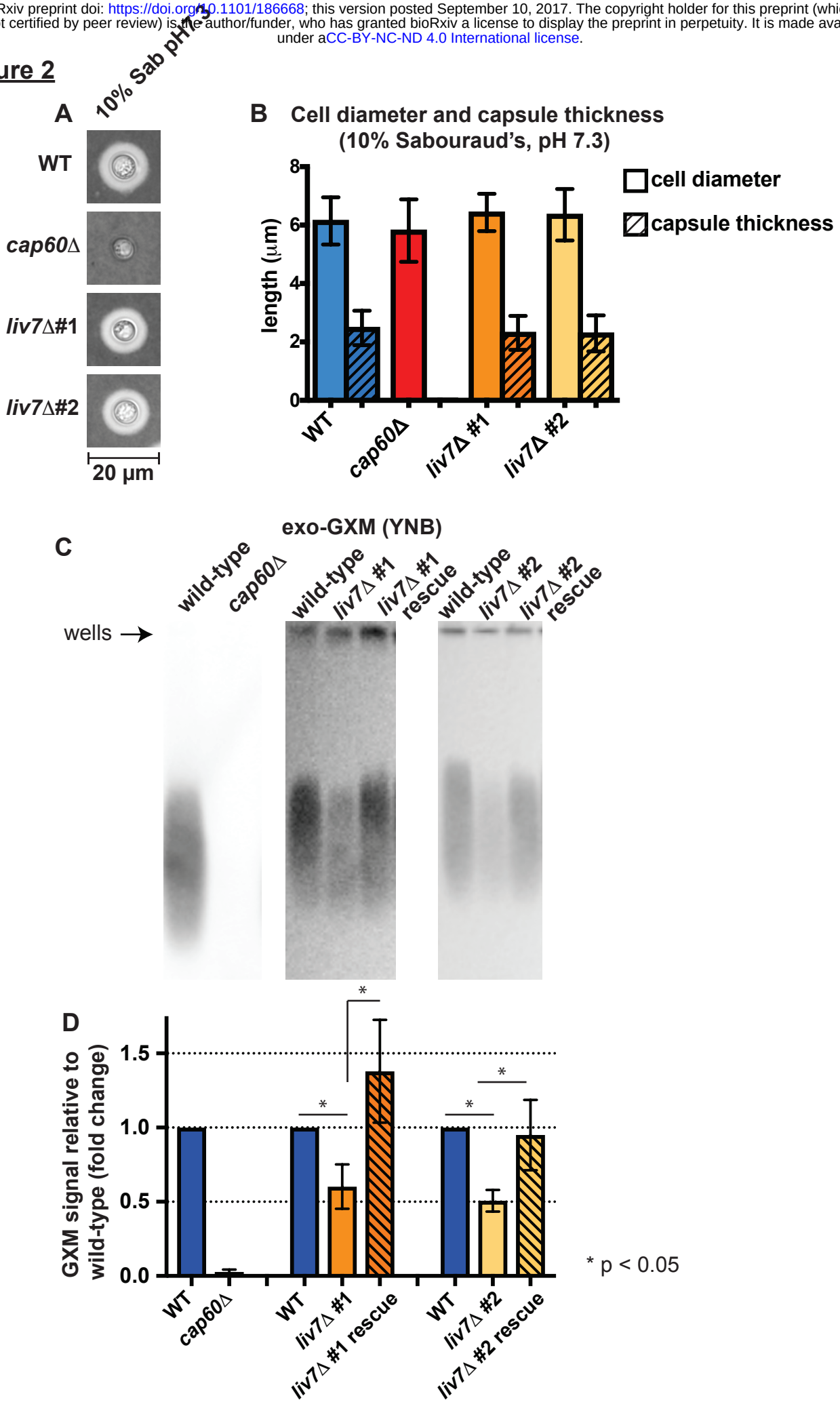

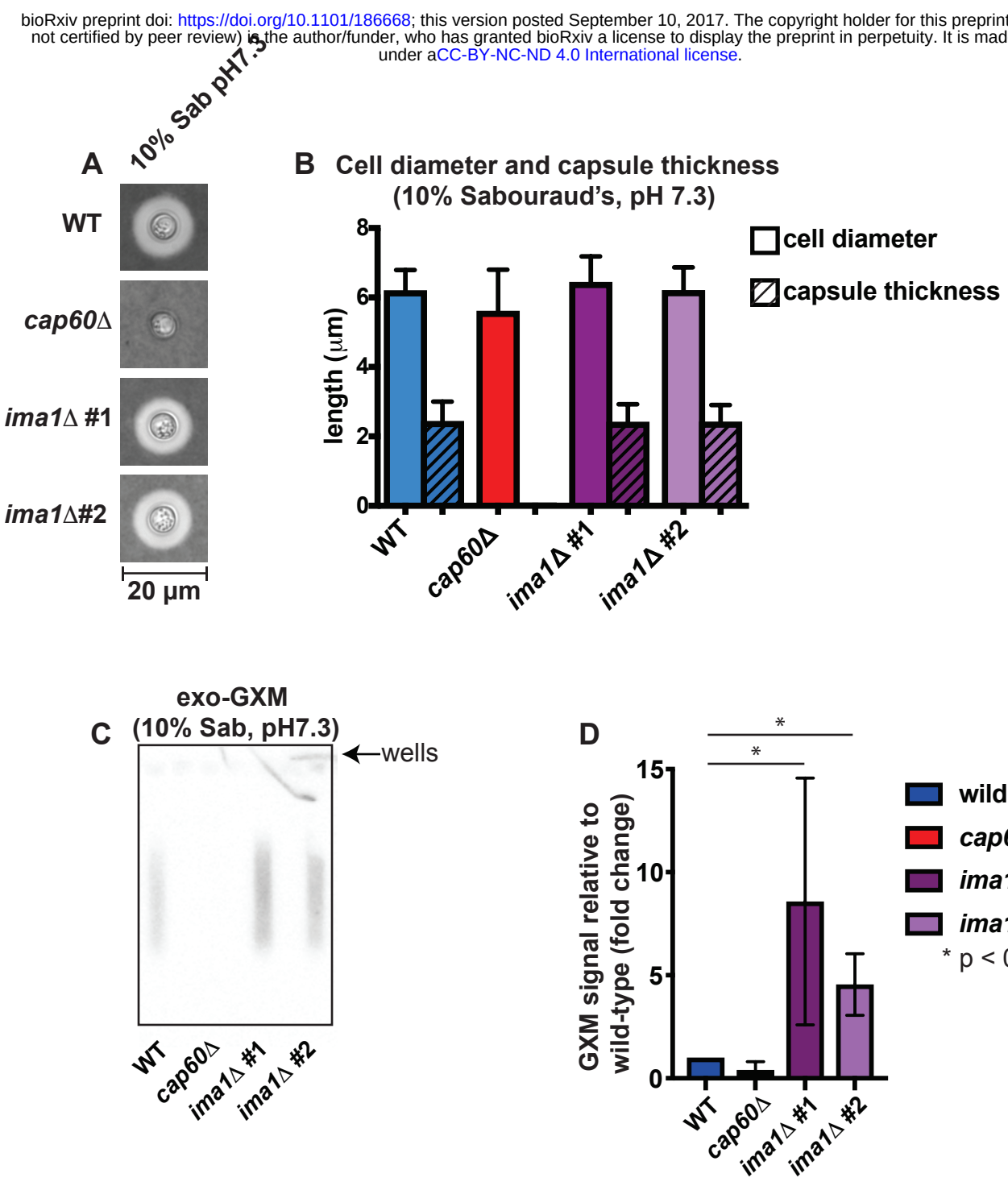

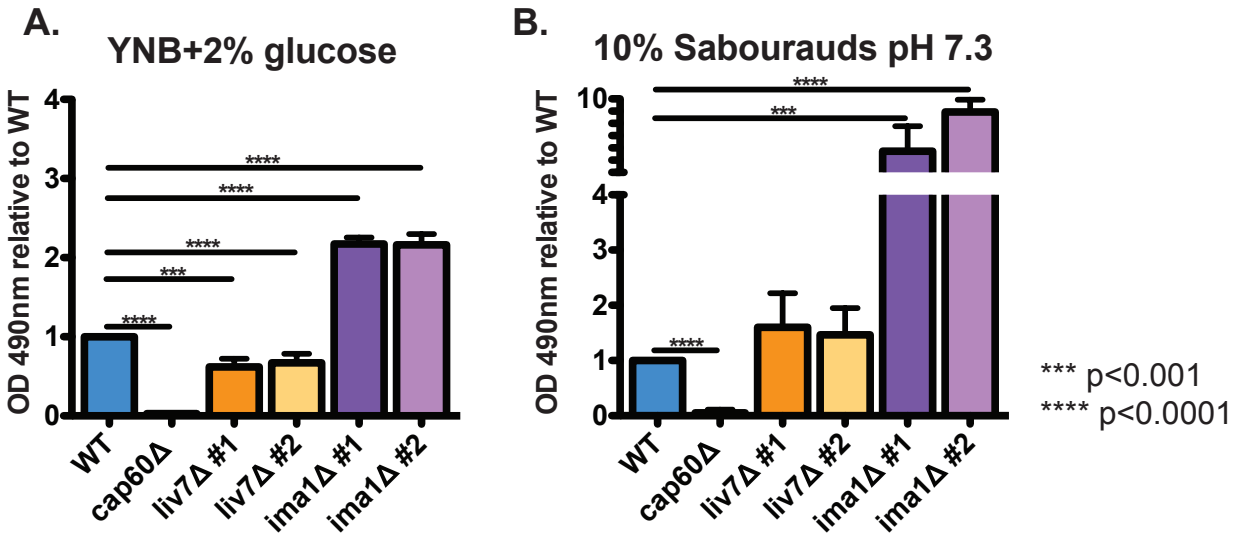

Figure 5

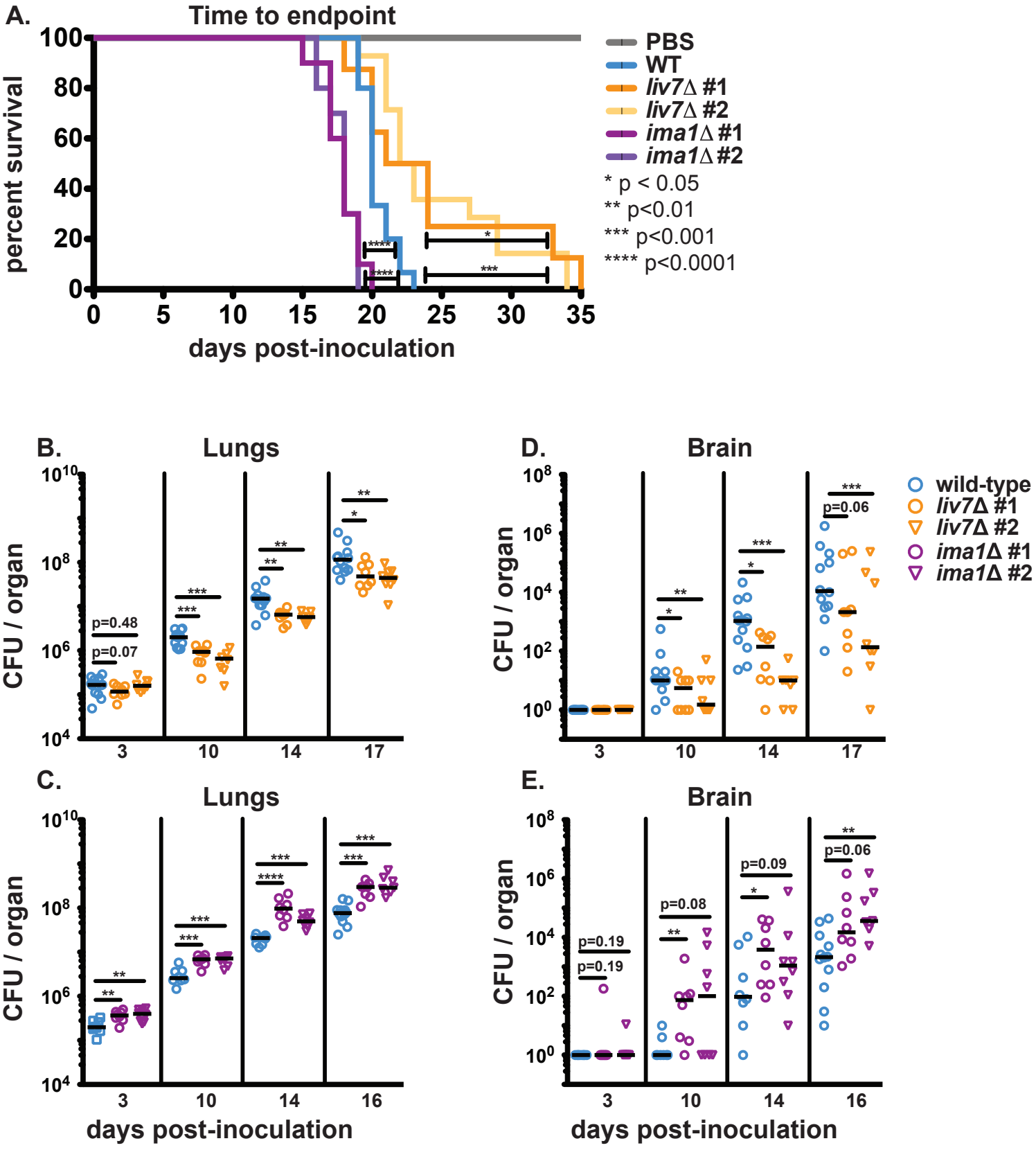

Figure 6

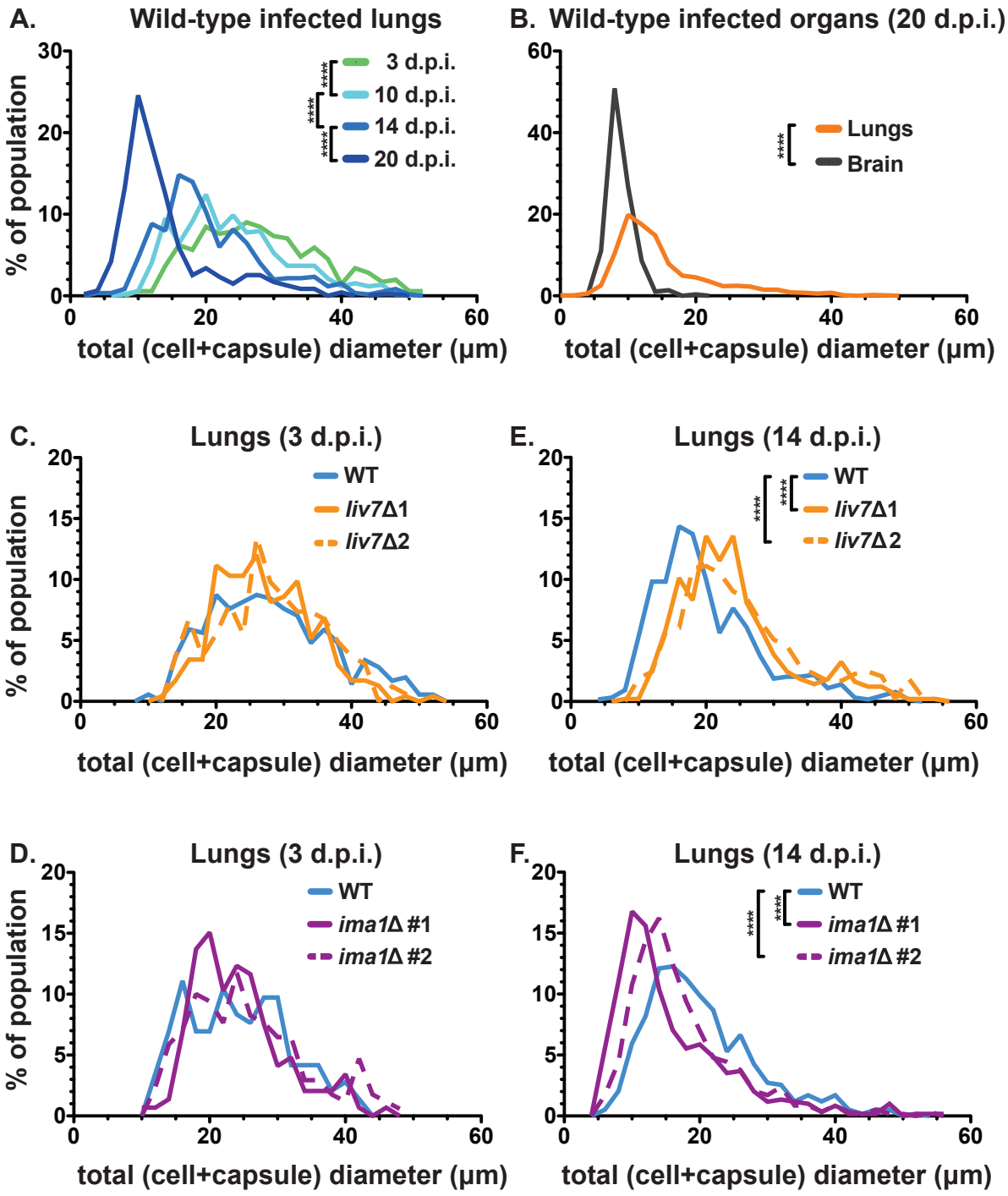

**** p < 0.0001

Figure 7

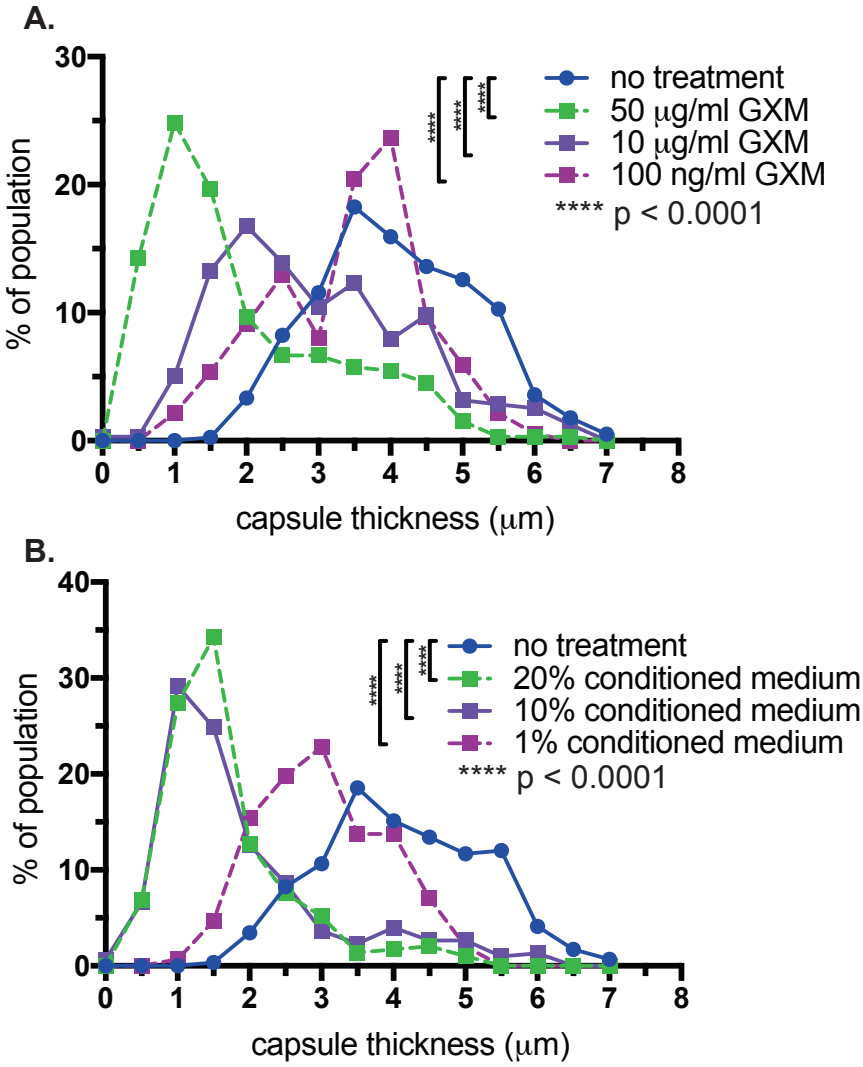

Figure 8

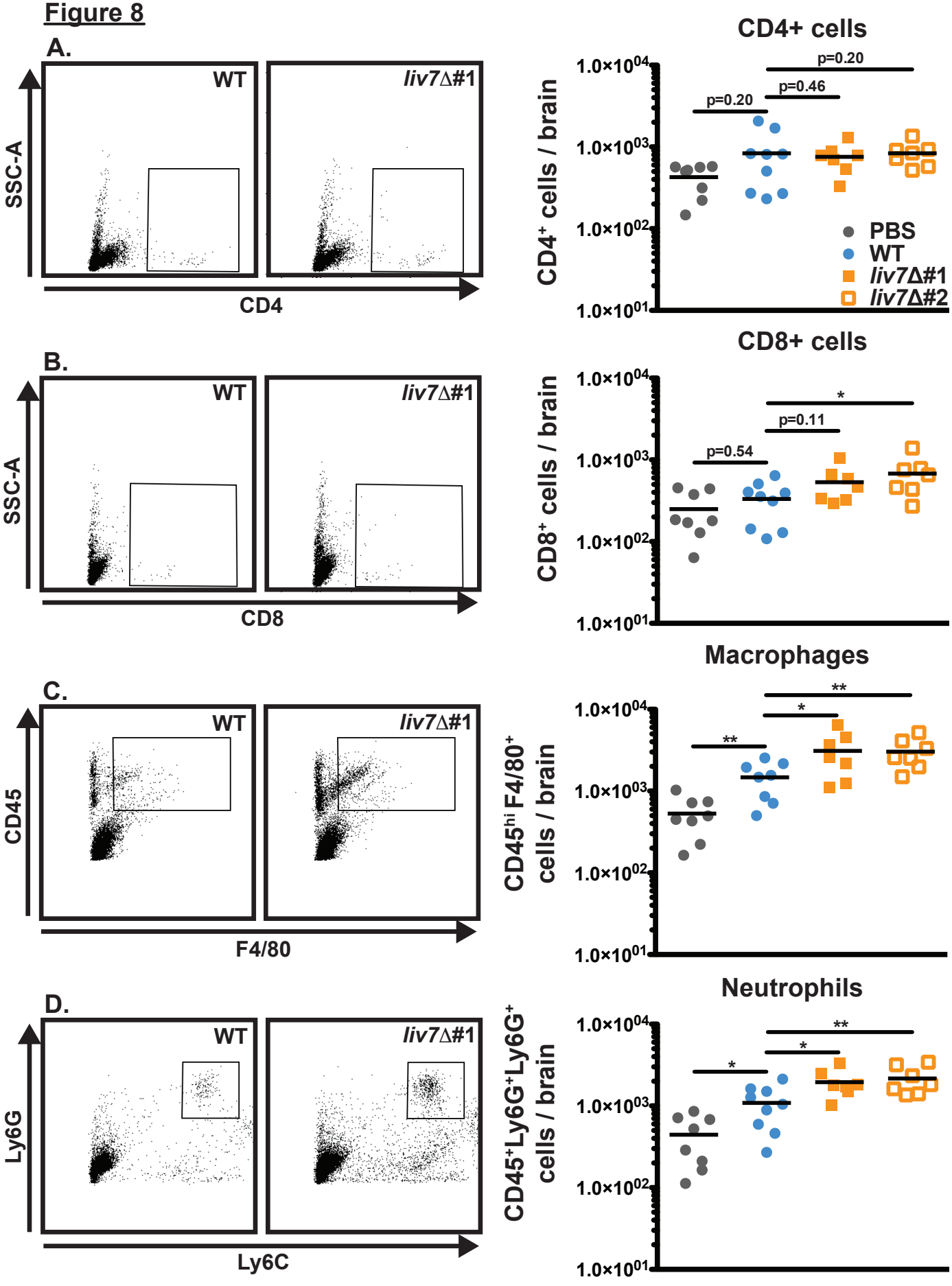

Figure 9

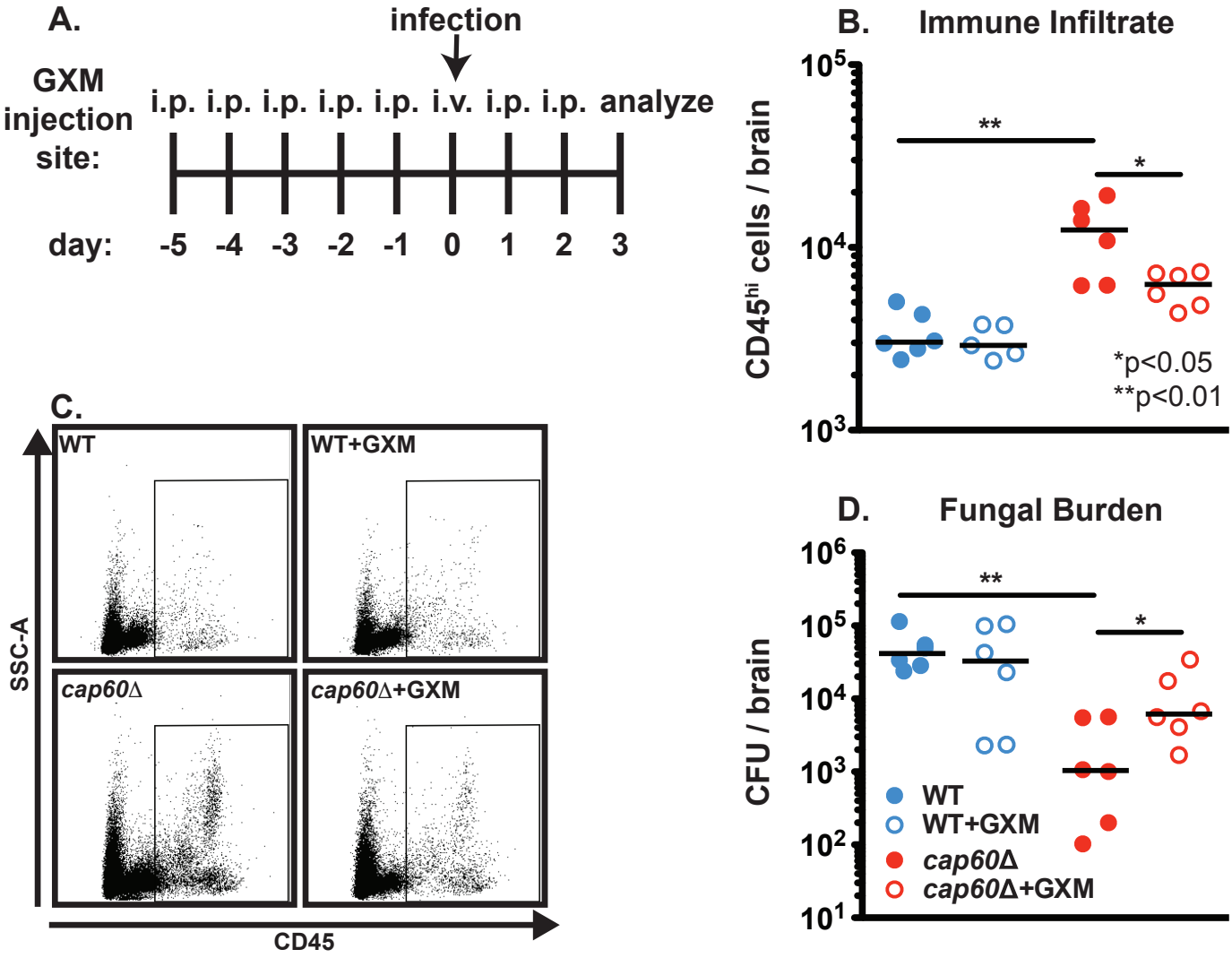

Figure S1

A. F12D2

O-acetyl (+) GXM binding

O-acetyl (-) GXM binding

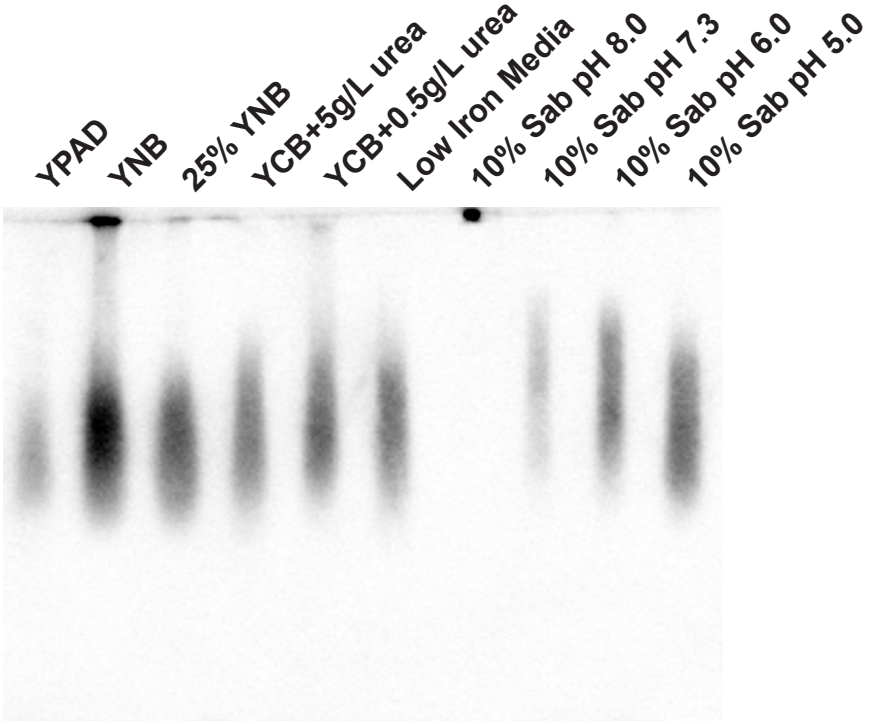

B. 1326

O-acetyl (+) GXM binding

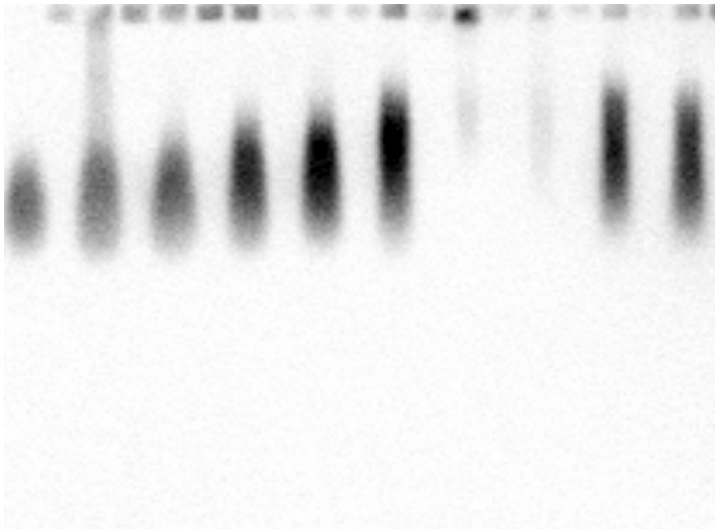

Figure S2

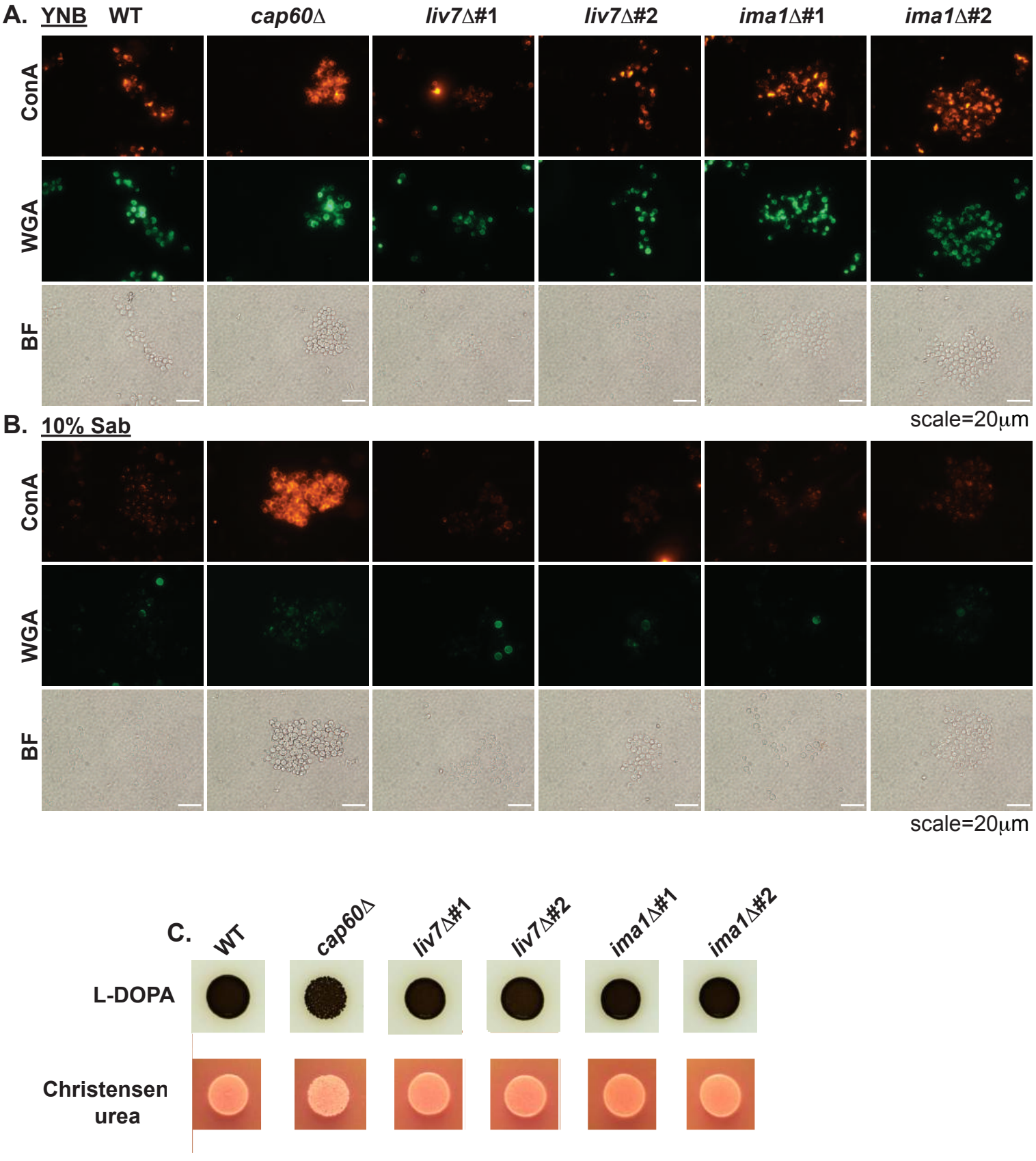

Figure S3

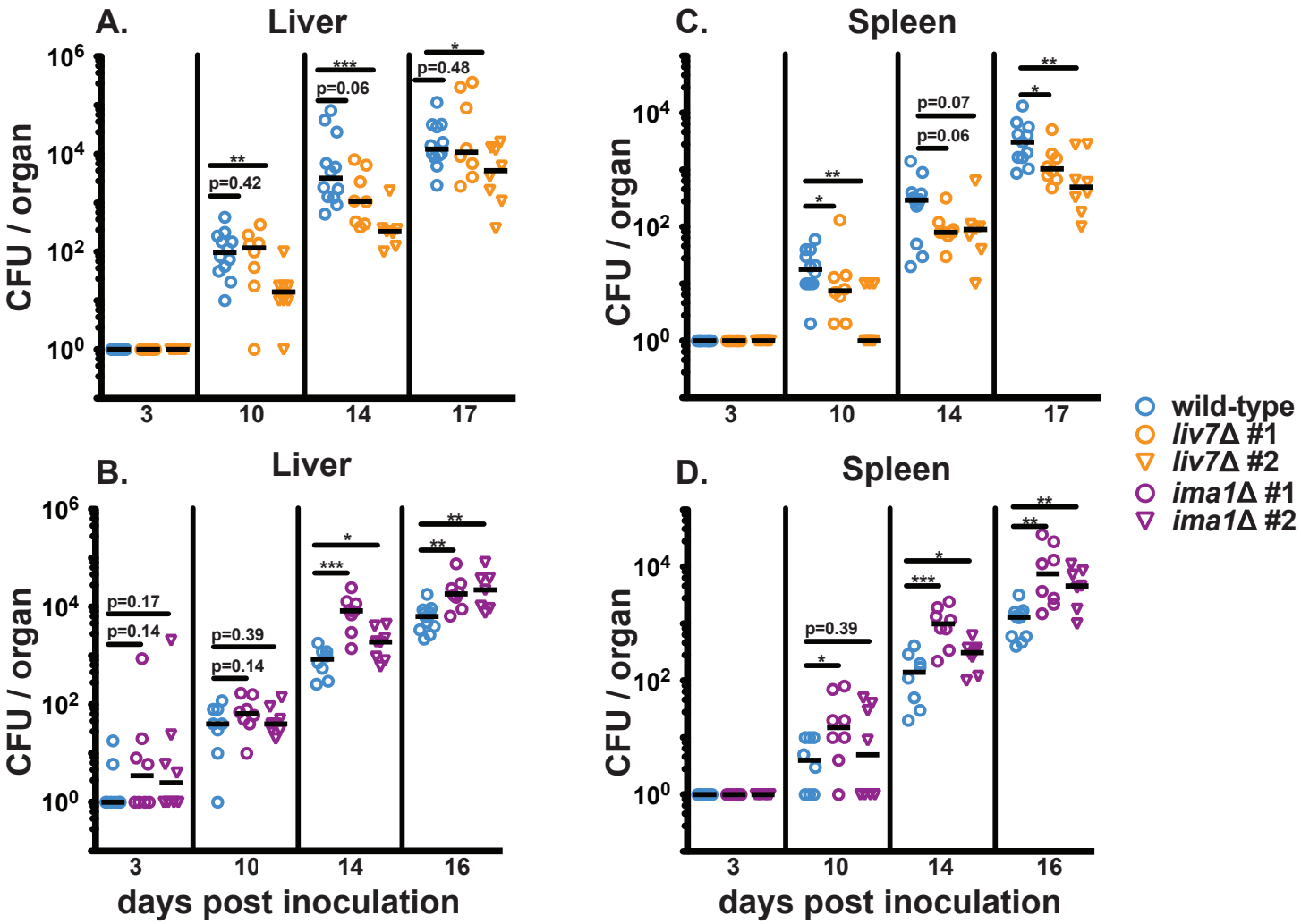

Figure S4

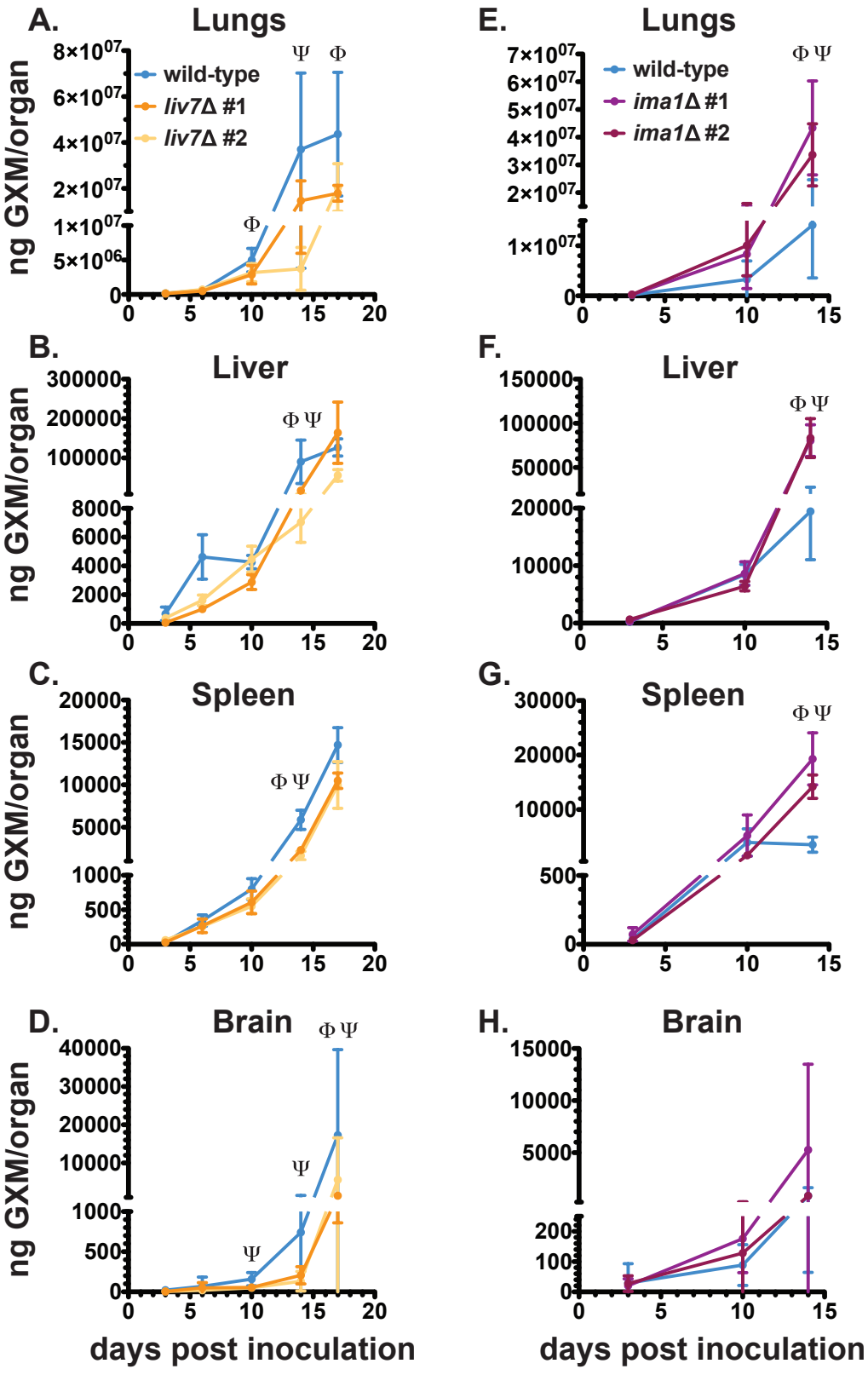

Φ p<0.05 (wild-type versus independent ko #1)
Ψ p<0.05 (wild-type versus independent ko #2)

Figure S5

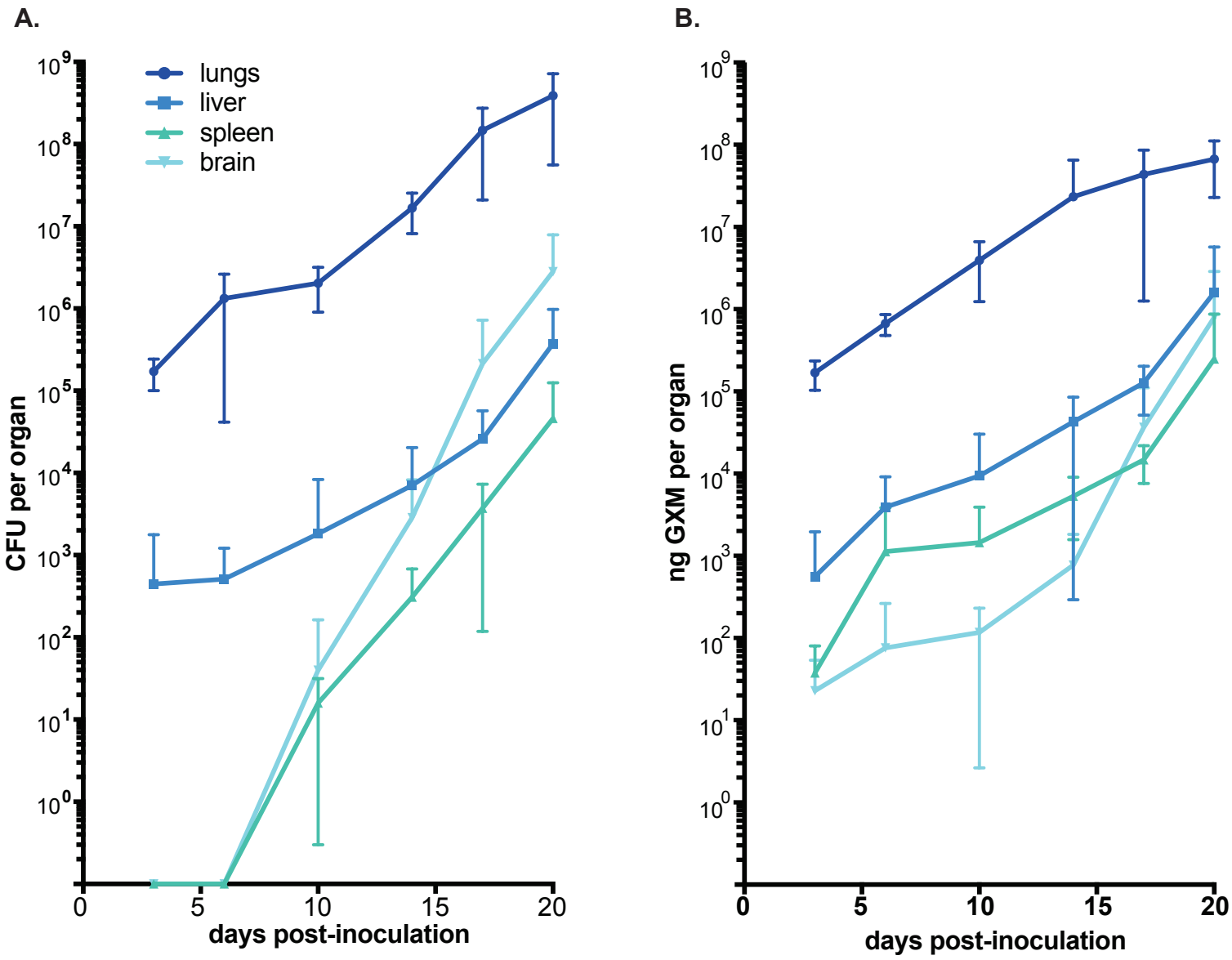

Figure S6

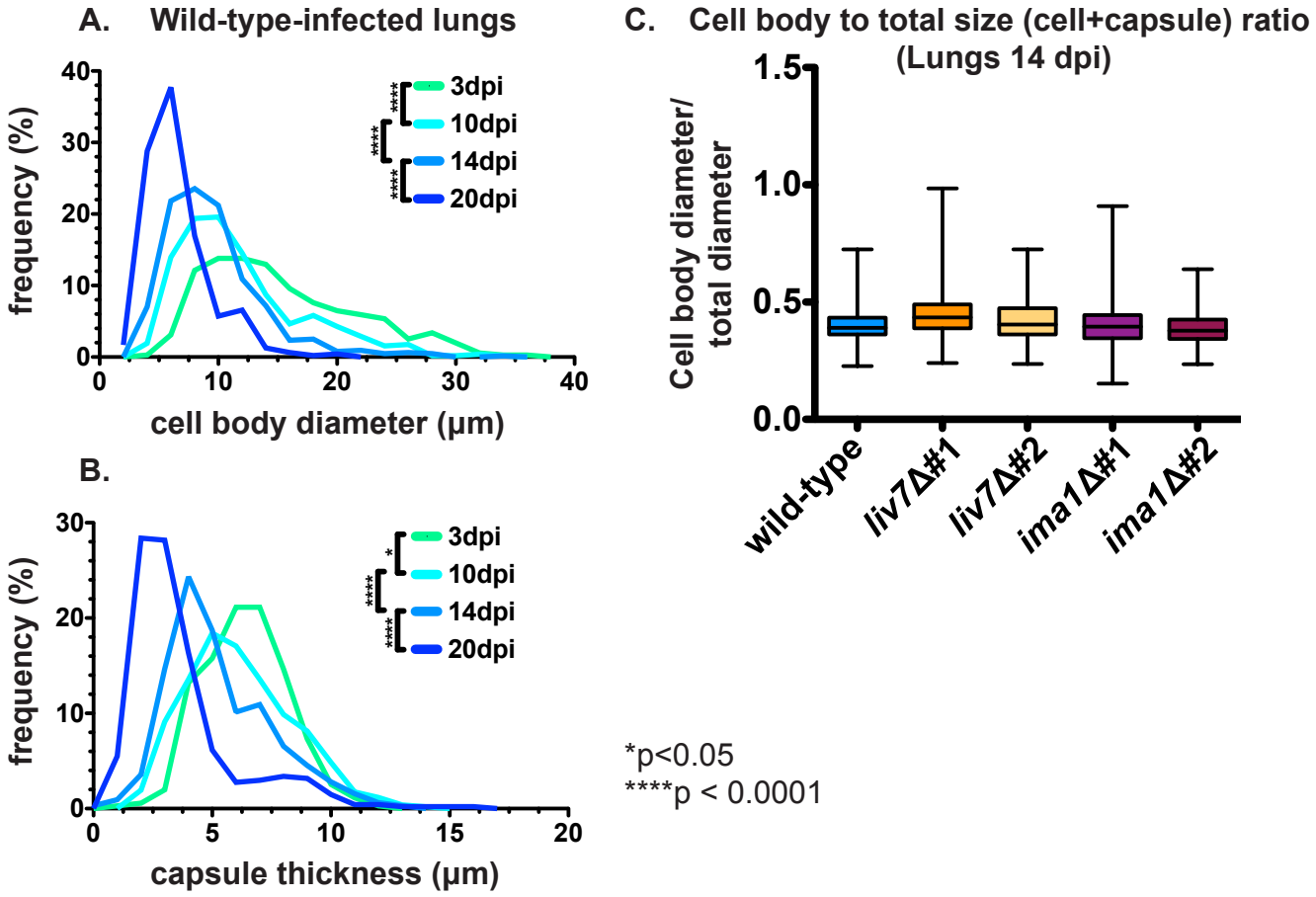

*p<0.05
****p < 0.0001

Figure S7

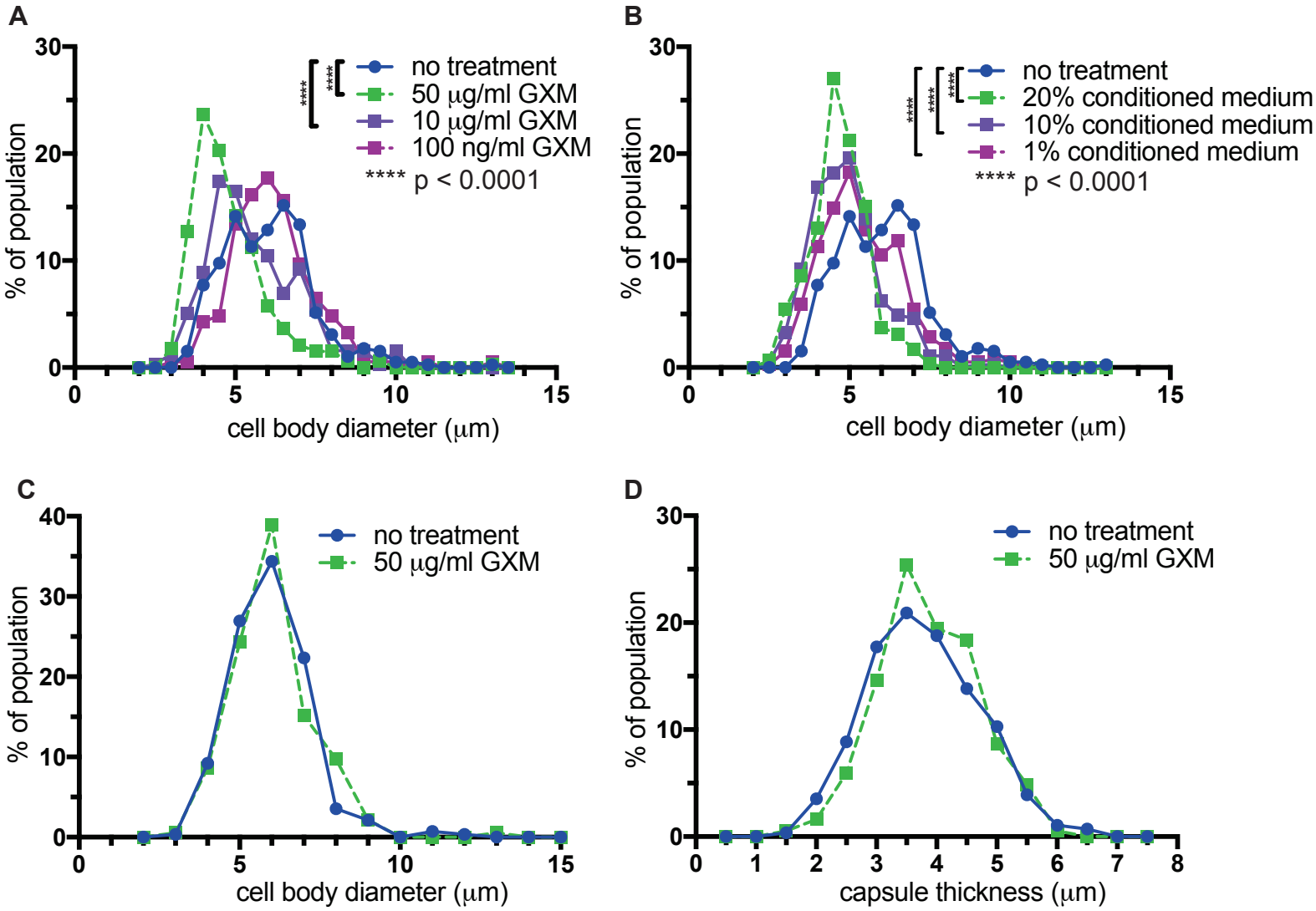

Figure S8

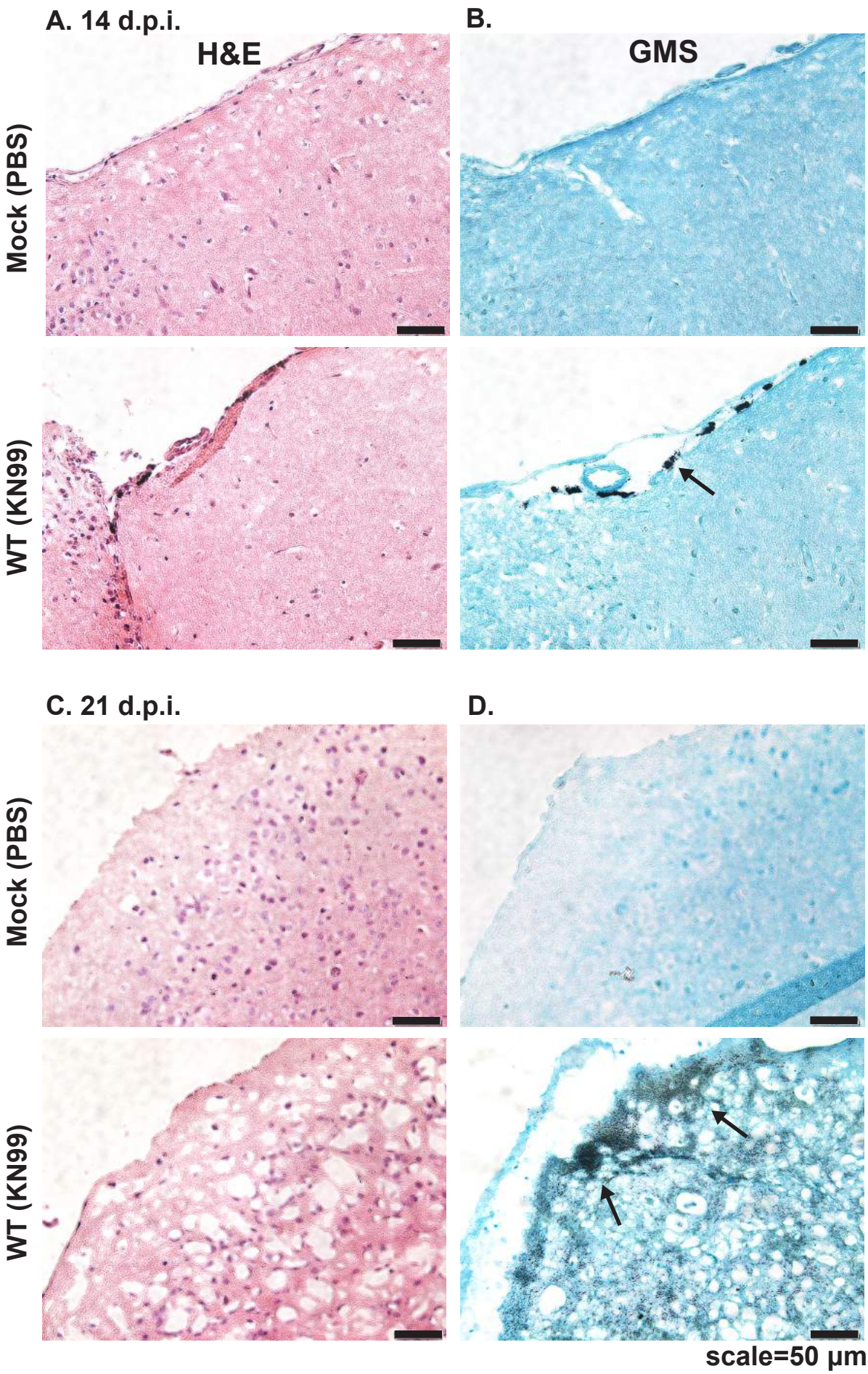

Figure S9

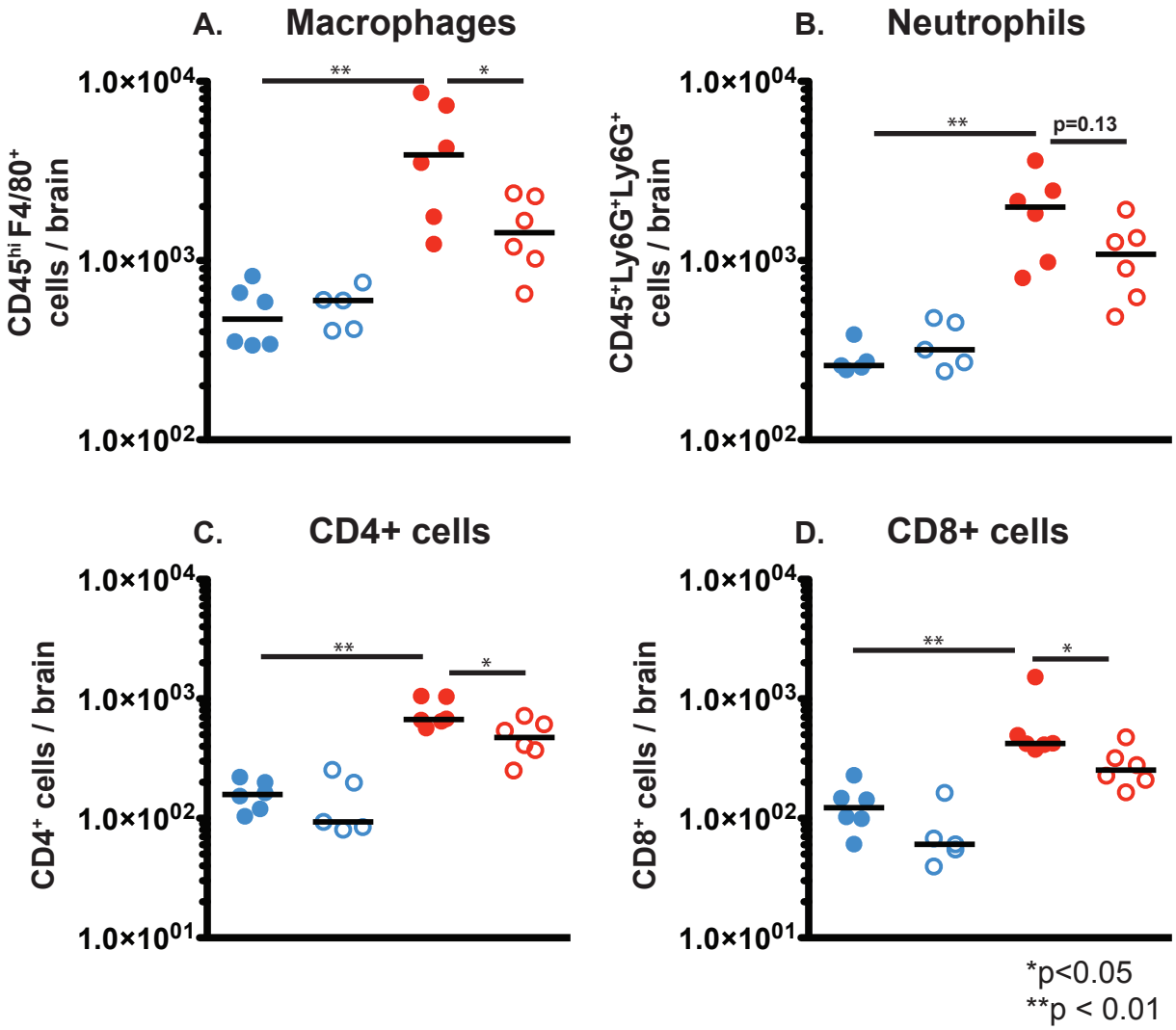

(A) Gene deletion mutants with reduced exo-GXM in YNB		
CNAG	**Molecular Function**	**Capsule**
CNAG_03171	WEE protein kinase	WT (++)
CNAG_04461	DNA helicase	++
CNAG_06673	conserved hypothetical protein	++
CNAG_04262	E3 ubiquitin-protein ligase (NRDP1)	++
CNAG_04443	conserved hypothetical protein	++

(B) Gene deletion mutants with increased exo-GXM in 10 Sabouraud's, pH 7.3					
CNAG	**Mutant Class**	**Molecular Function**	**Capsule**	**Urease**	**L-DOPA**
CNAG_00658	1	hypothetical protein	WT (++)	WT (++)	WT (++)
CNAG_03188	1	histone-lysine N-methyltransferase SETD2	++	++	-/+
CNAG_05838	1	Rho GTPase activating protein	+++	++	+++
CNAG_02189	1	alpha-amylase	++	++	++
CNAG_04756	1	hypothetical protein	++	++	++
CNAG_01551	2	transcription factor (Gat201)	-/+	++	++
CNAG_03582	2	pH response regulator protein (Rim20)	-/+	+++	-/+
CNAG_00375	2	histone acetyl transferase	-/+	++	-/+
CNAG_05690	2	histone deacetylase (Rpd3)	-/+	++	++
CNAG_04863	2	ESCRT-II complex subunit (Vps25)	-/+	+++	-/+
CNAG_03202	2	adenylate cyclase	-	++	-/+
CNAG_00761	2	coiled-coil domain-containing protein	+	+++	-/+
CNAG_06606	2	Rho family protein	+	+++	+
CNAG_05901	2	hypothetical protein	+	+	-/+
CNAG_02215	2	transcriptional activator (Hap3)	+	+	-/+